



**Eight National Aerospace Conceptual Design Competition
(NACDeC-VIII)**

Final Design Report

Submitted by

College Name	Indian Institute of Technology Kanpur
Team Name	Team Prahaar
Team Leader Name	Joisar Priyesh Jitendra
Team Member 2	Shobhit Sharma
Team Member 3	Dharshan S Hegde
Team Member 4	Arushi Gupta

Under the guidance of

Prof. G.M. Kamath



June 25, 2025

Certificate

It is certified that this Final Design Report of team: **Prahaar** is approved by me for submission. Certified further that, to the best of my knowledge, the report represents work carried out by the students.



Dr. G M Kamath

Signature and Name of Faculty Mentor

Date: 25 June 2025

डॉ जी० कम० कामथ
Dr. G.M. Kamath
प्रोफेसर एंड विभागाध्यक्ष
Professor & Head
वार्तिक अभियानिकी विभाग
Department of Aerospace Engg.
भारतीय प्रौद्योगिकी संस्थान, कानपुर
Indian Institute of Technology
कानपुर - 208016
Kanpur, India-208 016

ABSTRACT

The design of a Supersonic Unmanned Combat Aerial Vehicle (SUCAV) entails complex multidisciplinary trade-offs, particularly in optimizing aerodynamic performance across both supersonic and subsonic flight regimes while ensuring robust stability and control. This study addresses these challenges through the development and implementation of a comprehensive, open-source-based design and optimization framework.

The wing geometry was developed and parameterized using OpenVSP, which enabled flexible and efficient geometric manipulation. Low-fidelity aerodynamic analysis was conducted using FlightStream, employing a panel method capable of capturing flow characteristics in both subsonic and supersonic regimes. The optimization process was managed within the OpenMDAO framework, which allowed seamless integration of geometry generation, aerodynamic analysis, weight estimation, and performance evaluation within a unified, iterative loop. The optimization objective centered on maximizing a custom-defined flight performance metric, termed the flight score.

A gradient descent algorithm was employed to iteratively refine key wing design variables, aiming to enhance aerodynamic efficiency and overall mission performance. Multiple off-the-shelf NACA supersonic airfoils were evaluated within this framework, and the final wing configuration was selected based on the highest flight score achieved.

Following the selection of the optimal configuration, detailed analyses were conducted to assess aerodynamic performance, weight characteristics, stability behavior, and propulsion sizing. The aircraft exhibited consistent performance across flight regimes and satisfied key stability criteria, particularly at supersonic speeds. In parallel, structural analysis, including internal wing structure development and material selection, was carried out and validated using V-n diagram.

Overall, the results validate both the robustness of the proposed methodology and the fidelity of the integrated tools used within the framework. The approach successfully demonstrated a streamlined workflow for conceptual SUCAV design, with the flexibility to be extended in future studies for higher-fidelity modelling.

Acknowledgements

We, the authors, would like to express our sincere gratitude to **Prof. G. M. Kamath** and **Prof. Abhishek** for their invaluable guidance, insightful suggestions, and continuous support throughout the course of this project. Their mentorship has been crucial in shaping our understanding and approach.

We are also thankful to the **Department of Aerospace Engineering, IIT Kanpur**, for providing the direction, resources, and a vibrant academic environment that enabled us to carry out this work effectively.

This project would not have been possible without the support, infrastructure, and encouragement provided by **IIT Kanpur**, and we gratefully acknowledge the institution's role in fostering innovation and excellence.

Contents

Acknowledgements	iv
List of Figures	viii
List of Tables	x
Abbreviations	xi
Symbols	xiii
1 Introduction	1
1.1 Background	1
1.2 Motivation	1
1.3 Mission Profile and Objectives	2
1.3.1 Mission Requirements	3
1.4 Organization of the Report	3
1.5 Details of Tools used :	4
1.6 Literature Survey	5
1.6.1 Configuration Selection :	5
1.6.2 Review for Performance and Stability Analysis	6
2 Design Framework	7
2.1 Key Design drivers	7
2.1.1 Analytical Heirarchy Process (AHP)	9
2.1.2 Potential Vehicle Configuration	9
2.1.3 Pugh Matrix	10
2.2 Initial Sizing	11
2.2.1 Constrain analysis	11
2.2.2 Weight Estimation	12
2.2.2.1 Empty Weight Estimation	13
2.2.2.2 Fuel Weight Estimation by Mission Segments	13
2.2.2.3 Total Fuel Weight (with Reserves)	13
2.2.2.4 Iteration for Final Takeoff Weight	14

2.2.2.5	Weight Breakdown	14
2.2.3	Engine Selection	14
2.2.4	Airfoil Selection	16
2.3	Multidisciplinary Design Analysis and Optimization	17
2.4	Final Design	18
2.4.1	Wing	18
2.4.2	Payload Bay	20
2.4.3	Fuselage	21
2.4.4	Final Design	23
2.4.5	Engine Inlet	24
3	Aerodynamic Analysis	26
4	Performance and Stability Analysis	29
4.1	Background	29
4.2	Performance Evaluation	30
4.2.1	Range Evaluation	30
4.2.2	Level Turn	30
4.2.3	Gliding Flight	32
4.2.4	Thrust - Drag Comparison at Specific Altitudes	33
4.2.5	Energy Maneuverability Methods	34
4.2.5.1	P_s vs M	36
4.2.5.2	Alt vs M	36
4.2.5.3	P_s vs Ψ	37
4.2.6	Minimum Time To Climb	37
4.2.7	Takeoff Performance	40
4.2.8	Landing Performance	41
4.3	Flight Score	42
4.4	Stability Analysis	42
4.4.1	Aerodynamic Parameters	42
4.4.2	Static Stability	42
4.4.2.1	Longitudinal Stability	42
4.4.2.2	Directional Stability (Weathercock Stability)	45
4.4.3	Dynamic Stability	45
4.4.3.1	Longitudinal Modes	45
4.4.3.2	Lateral-Directional Modes	47
5	Structures and Loads	49
5.1	Introduction	49
5.2	Loading	49
5.3	Material Selection and Thermal Considerations	52
5.4	Wing Structure	52
6	Propulsion Sizing	55
6.1	Background	55

6.2	Engine Sizing	55
6.3	Cycle Analysis	56
7	Radar Cross Section(RCS)	58
7.1	Background	58
7.2	RCS Analysis	58
8	Conclusion	60
 Bibliography		 61

List of Figures

1.1	Mission Profile of SUCAV	3
1.2	Different Configurations of Aircrafts	5
2.1	Radar Plot	10
2.2	Constrain Analysis	12
2.3	Powerplant selection	15
2.4	Thrust vs mach number	16
2.5	Supersonic airfoil comparision	17
2.6	Wing design MDAO algorithm	18
2.7	Final wing 3 view	19
2.8	Payload Bay Configuration in OpenVSP	21
2.9	Fuselage and Payload Bay Integration in OpenVSP	22
2.10	Final Design in OpenVSP	23
2.11	Figure: Basic Dimensions	23
2.12	Variable Inlet Geometry	24
2.13	Inlet Selection Criteria	25
2.14	Upper Fuselage Inlet	25
3.1	Aerodynamic data (Alpha Sweep) for subsonic and supersonic	27
3.2	Aerodynamic data (Beta Sweep) for supersonic	27
3.3	Drag Divergence and L/D vs Mach number	28
3.4	Mach Contour	28
3.5	Pressure Contour	28
4.1	Range vs Speed at Various Altitudes	30
4.2	Turn Characteristics During Loiter	31
4.3	Turn Characteristics During Cruise	31
4.4	Sink Rate with Speed (Cruise) at 100% Weight	32
4.5	Sink Rate with Speed (Cruise) at 50% Weight	33
4.6	Glide Angle with Speed (Cruise) at 100% Weight	33
4.7	Glide Angle with Speed (Cruise) at 50% Weight	34
4.8	Thrust Profile at Cruise Altitude	34
4.9	Thrust Profile at Loiter Altitude	35
4.10	Ps vs M at Cruise Altitude	37
4.11	Ps vs M at Loiter Altitude	37
4.12	Alt vs M, Ps=0	38

4.13 Alt vs M, n=1	38
4.14 Ps vs Ψ , $M = 0.9$, $Alt = 9000m$	39
4.15 Ps vs Ψ , $M = 0.5$, $Alt = 1500m$	39
4.16 Climb Path from Takeoff to Cruise	40
4.17 Climb from Loiter to Cruise	41
4.18 Trim Conditions	44
4.19 Phugoid Mode	46
4.20 Short Period Mode	46
4.21 Spiral Divergence Mode	47
4.22 Roll Mode	48
4.23 Dutch Roll Mode	48
 5.1 V-n diagram	50
5.2 Shear Force Diagram	51
5.3 Bending Moment Diagram	51
5.4 Temperature distribution at different altitudes to mach number	53
5.5 Predicted equilibrium skin temperatures for Mach 2.2 and 2.4 SCT aircrafts	53
5.6 Converging Spars [19]	54
5.7 Wing Structure	54
 6.1 Engine Cycle	56
6.2 Component efficiency	57
 7.1 Monostatic RCS v/s Azimuth Angle	59

List of Tables

1.1	Mission Requirements	3
1.2	Aircraft Performance Comparison	5
2.1	Analytical Heirarchy Process	9
2.2	Design Driver Evaluation	10
2.3	Aircraft Weight Breakdown	14
2.4	Weight Fractions	14
2.5	NACA 64A Series Airfoil Characteristics	17
2.6	Wing Parameters	19
2.7	Payload Dimensions	20
2.8	Payload Bay Dimensions	20
3.1	Atmospheric data at 14 km Altitude	26
4.1	Vehicle Performance Parameters	42
5.1	Material properties of aircraft structural components	53
6.1	Comparative Performance Specifications of Jet Engines	56

Abbreviations

SUCAV	Supersonic Unmanned Combat Aerial Vehicle
UAV	Unmanned Aerial Vehicle
UCAV	Unmanned Combat Aerial Vehicle
IRA	Indian Reference Atmosphere
MDO	Multidisciplinary Design Optimization
AR	Aspect Ratio
MAC	Mean Aerodynamic Chord
RCS	Radar Cross Section
IR	Infrared
AoA	Angle of Attack
L/D	Lift-to-Drag Ratio
TWR	Thrust-to-Weight Ratio
VSP	Vehicle Sketch Pad
CG	Center of Gravity
CM	Pitching Moment Coefficient
SFC	Specific Fuel Consumption

L/D	Lift-to-Drag Ratio
CG	Center of Gravity
CL	Lift Coefficient
CD	Drag Coefficient
Cm	Moment Coefficient
FS	Flight Stream
VSPAERO	OpenVSP's Aerodynamic Solver

Symbols

W_0	Gross Takeoff Weight	kg
W_e	Empty Weight	kg
W_f	Fuel Weight	kg
W_{payload}	Payload Weight	kg
S_{ref}	Reference Wing Area	m^2
b	Total Wingspan	m
c_{mac}	Mean Aerodynamic Chord	m
c_{root}	Root Chord	m
c_{tip}	Tip Chord	m
Λ_{TE}	Trailing Edge Sweep Angle	degrees
ϕ	Twist	degrees
Γ	Dihedral Angle	degrees
AR	Aspect Ratio	—
λ	Taper Ratio	—
P	Pressure	Pa
T	Temperature	K
ρ	Air Density	kg/m^3
a	Speed of Sound	m/s
μ	Dynamic Viscosity	$\text{Pa}\cdot\text{s}$
R	Gas Constant	$\text{J}/(\text{kg}\cdot\text{K})$
γ	Ratio of Specific Heats	—
T	Total Thrust	N
F	Fuel-to-weight Ratio	—

u_e	Exit Velocity	m/s
u	Inlet Velocity	m/s
P_e	Exit Pressure	Pa
P_a	Ambient Pressure	Pa
A_e	Nozzle Exit Area	m ²
L/D	Lift-to-Drag Ratio	—
M	Mach Number	—
C	Specific Fuel Consumption	1/s
E	Loiter Time	min
R	Range	km

Chapter 1

Introduction

1.1 Background

SUCAV, also known as Supersonic Unmanned Combat Aerial vehicle, is an advanced drone designed to operate at speeds greater than Mach 1. It is used to perform high speed combat missions, precision strikes and reconnaissance missions without involving of human pilots. The key requirements for such a system involve advanced stealth technologies, high manoeuvrability to evade enemy defences and supersonic propulsion. Traditional UCACV's typically in the region of subsonic or low supersonic faces limitations when operating in high threat environments or areas defended by advanced air defence systems. To counter these threats/challenges the concept of SUCAV (Supersonic Unmanned Combat Aerial vehicle) has emerged. The SUCAV's are still in the developmental phase in many countries with multiple organizations exploring potential segments for high-speed, high-risk operations. They are seen as the future of combat especially as tensions increase in regions with advanced anti-aircraft and missile defence systems.

1.2 Motivation

The core motivation behind the development of SUCAV's stems from evolving military needs and the growing complexity of modern warfare. With advancements in radar, missile technology and electronic warfare traditional manned aircraft are facing several challenges in penetrating defended airspace without being intercepted or detected, SUCAV's provide

a potential solution to this problem enabling to carry out strategic strikes and reconnaissance mission. NACDeC-VIII competition focuses on the conceptual design and sizing of Supersonic Unmanned aerial vehicle and aims to identify feasible designs of UAV.

1.3 Mission Profile and Objectives

The SUCAV (Supersonic Unmanned Combat Aerial Vehicle) is designed for rapid deployment in high-threat environments, performing reconnaissance, surveillance, and tactical engagements. Emphasis is placed on long-range operations and sustained supersonic flight capability at varying altitudes.

The mission profile consists of 8 segments, as illustrated in Figure ??:

1. **Take-off and Climb:** Ascend to an altitude of 14 km.
2. **Onward Cruise:** Maintain a minimum Mach number of 2.3 to ensure the mission is completed in under 1 hour.
3. **Ingress:** Transition from supersonic to subsonic flight and descend to an altitude of 1.5 km.
4. **Strike:** Loiter briefly and release payload. A loiter time of 3 minutes is assumed according to /cite.
5. **Egress:** Transition back to supersonic and ascend to 14 km for the return phase.
6. **Return Cruise:** Maintain Mach 2.3 for efficient return within 1 hour total flight time.
7. **Descent and Landing:** Land on a 2000-meter runway.

With the defined mission profile, the SUCAV must be optimized for performance across all flight segments, ensuring rapid transit and enhanced operational capability. Furthermore, the design must incorporate stealth considerations to minimize the aircraft's radar cross-section (RCS), infrared (IR) signature, and aural detectability.

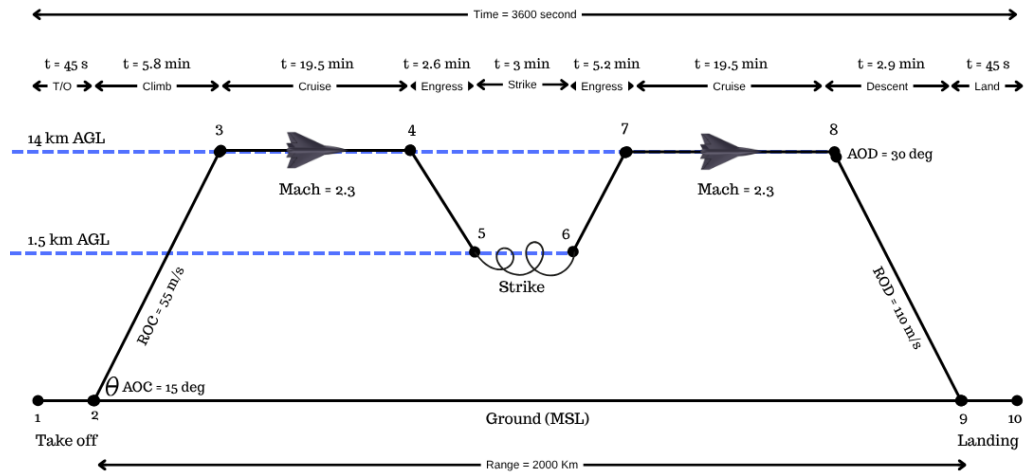


FIGURE 1.1: Mission Profile of SUCAV

1.3.1 Mission Requirements

The mission-specific requirements that govern the design of SUCAV are listed in Table 1.1.

TABLE 1.1: Mission Requirements

Parameter	Value	Unit
Payload Mass	≥ 1000	kg
Range (Take-off to Strike Location)	≥ 1000	km
Total Mission Time	≤ 1	hour
Take-off Distance	≤ 2000	m
Landing Distance	≤ 2000	m
Change in Static Margin (Sub → Supersonic)	$\leq +10\%$	—
Atmospheric Model	Indian Reference Atmosphere (IRA)	—

1.4 Organization of the Report

The report is organized into the following chapters:

- **Chapter 1:** Provides a basic introduction to SUCAV, outlining the mission profile, objectives, requirements, literature survey of existing technologies, and details of the tools/software used.

- **Chapter 2:** Provides a detailed literature survey on configuration, design, performance, etc.
- **Chapter 3:** Describes the design framework and sizing algorithm and initiates the design process, including optimization of the complete UAV configuration along with weight estimation and final design of the UCAV
- **Chapter 4:** Covers the aerodynamic analysis carried out in both subsonic and supersonic flight regimes.
- **Chapter 5:** Focuses on Performance and stability analysis of the UCAV .
- **Chapters 6 & 7:** Detail the selection of the material ,loading acting and finally the design of wing internal structure . It also discusses the engine sizing for the same
- **Chapters 8:** Present the RCS calculation and methods for stealth for an UCAV.

1.5 Details of Tools used :

- **Open VSP:** It is an aircraft design tool widely used in the aircraft industry, developed by NASA. It uses the Plot3D format to model the aircraft body. A low-fidelity panel method is also included for quick aerodynamic analysis. As it is a panel code, the flow is inviscid, and there is no stall prediction in this tool. For this reason, we use this tool to create the aircraft body, and the aerodynamic analysis is carried out in Flight Stream software [1].
- **Flight Stream:** It is a medium-fidelity surface vorticity panel code with viscous correction, capable of predicting the stall region. Details of the Flight Stream software can be found in the work of Ahuja. For supersonic flow, an inviscid low-order solver is used. It employs the Prandtl-Glauert compressibility correction method to calculate aerodynamic loads at supersonic speeds [2].
- **Open MDAO:** A Python-based open-source multidisciplinary design optimization (MDAO) framework. It offers many optimization techniques that can be integrated with our design framework to generate an optimized wing. For the current study, we are using the gradient descent approach [3].

1.6 Literature Survey

1.6.1 Configuration Selection :

The mission statement mentions the design of a UCAV capable of carrying a payload of 1000 kg and a supersonic aircraft with stealth capabilities .Considering these factors a wide range of design options/configurations were considered given below :

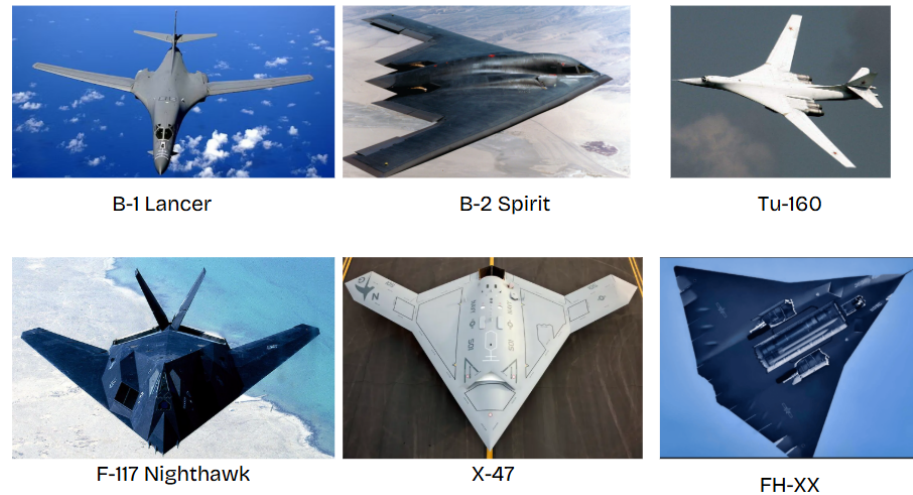


FIGURE 1.2: Different Configurations of Aircrafts

Additional list of surveying of existing fighter aircrafts and UCAV technologies, the list of aircrafts used for literature survey are:

TABLE 1.2: Aircraft Performance Comparison

Aircraft	Engine	Alt. (m)	Speed (M)	T/W
F-22	2 × F-119-PW-100 Turbofans	18k	1.76 (SC) 2.25 (Max)	1.08
SR-71	2 × J58 Turbojets	24k	3.3	0.44
Concorde	4 × RR MK610 Turbojets	16.3k	2.04 (SC)	0.73
F-35	1 × F135 PW100 Turbofan	13k	1.6	0.87
Eurofighter	2 × EJ200 Turbofans	14.8k	1.5 (SC) 2.35 (Max)	1.15
Su-57	2 × AL-41F1 Turbofans	18k	1.3 (SC) 2.0 (Max)	1.09
Rafale	2 × M88-Ae Turbofans	13.8k	1.4 (SC) 1.6 (Max)	1.57

SC = Super Cruise, k = ×1000

1.6.2 Review for Performance and Stability Analysis

The performance analysis process follows the methodology provided by [4]. In addition to this book, the equations used for the analysis have been referred to in certain sections from [5]. The Oswald Span Efficiency is assumed to be 0.7 as referenced from [Aerodynamics Aeronautics and Flight Mechanics by McCormick]. The matching of Thrust with Respect to Mach No. has been done by following the methodology presented in [6] who in turn referred to [7].

Stability Analysis has been primarily based on the methods laid out by [Flight Stability and Automatic Control by RC Nelson][[8]]. In addition, the equations have been referred to in certain cases from [Dynamics of Flight by Bernard Etkins][[9]] and [10] Certain Assumptions for supersonic flight have been referred to from [4]

Chapter 2

Design Framework

2.1 Key Design drivers

Design drivers are the key performance parameters and critical factors that significantly influence the design, performance, and feasibility of a supersonic UCAV objectives. Detailed list and description of design drivers are explained below :

- **Aerodynamics Efficiency** : Aerodynamics efficiency refers to the aircraft's ability to generate optimal lift while minimizing drag, especially at supersonic speeds. It directly impacts fuel consumption, range, and overall L/D performance. Key considerations include shaping the airframe to reduce wave drag and optimizing wing design for high-speed stability. Efficient aerodynamics also enhance maneuverability, allowing the bomber to evade threats while maintaining speed and endurance.
- **Empty Fraction (Mass Efficiency)** : Empty fraction is the ratio of the aircraft's empty weight (without fuel or payload) to its maximum takeoff weight (MTOW). A lower empty fraction indicates a more structurally efficient design, allowing for greater fuel capacity or heavier payloads. This metric is crucial for long-range missions, as it determines how much weight can be allocated to weapons, sensors, or additional fuel. Advanced materials and weight-saving structural designs are key to optimizing this parameter.
- **Stealth Capabilities** : Stealth capabilities refer to the UCAV's ability to avoid detection by radar, infrared, acoustic, and electronic sensors. This involves shaping

the aircraft to minimize radar cross-section (RCS), using radar-absorbent materials (RAM), and managing heat signatures from engines. Effective stealth ensures survivability in contested airspace, enabling penetration of enemy defenses without being tracked. Advanced electronic warfare and signature suppression techniques further enhance low observability.

- **CG (Center of Gravity) Margin :** The CG margin defines the allowable range for the aircraft's center of gravity to maintain stable and controllable flight. A well-balanced CG is critical during fuel burn, payload release, and high-speed maneuvers. If the CG shifts outside acceptable limits, the aircraft may become unstable or difficult to control. Design considerations include fuel tank placement, weapon bay configuration, and control surface sizing to ensure dynamic stability across all flight conditions.
- **Ease of Transition (Between Flight Regimes) :** Ease of transition refers to the aircraft's ability to smoothly shift between subsonic, transonic, and supersonic speeds without performance penalties. This requires adaptive aerodynamics, such as variable-geometry inlets and wings, to manage shockwaves and airflow disruptions. Advanced flight control systems help automate transitions, reducing pilot workload. Efficient transition capability ensures fuel economy and operational flexibility during acceleration or deceleration.
- **Technological Readiness Level (TRL) :** TRL measures the maturity of critical technologies required for the aircraft's development, ranging from theoretical research (TRL 1) to fully operational systems (TRL 9). High TRL components reduce development risk, cost, and delays, while low-TRL innovations may introduce uncertainties. Key areas include propulsion systems, avionics, stealth materials, and weapon integration, each requiring validation before full-scale production.
- **Design Complexity :** Design complexity assesses the difficulty of integrating advanced systems while maintaining reliability, manufacturability, and maintainability. Highly complex designs may involve trade-offs between stealth, aerodynamics, propulsion, and avionics, increasing development time and cost. Simplifying subsystems, using modular designs, and ensuring supply chain resilience help mitigate risks associated with excessive complexity.

2.1.1 Analytical Heirarchy Process (AHP)

Design drivers were used for final vehicle selection. Each design driver was assigned a weight, representing the rank of importance relative to other drivers. The Analytic Hierarchy Process(AHP) [11] was used to determine the importance of each design driver. To remove bias, each group member constructed an AHP matrix with weights they deemed appropriate based on the RFP and mission profile. Each group member complied with a consistency index to ensure weights were not assigned randomly. Then, the mean values for the weights were calculated while ensuring a low standard deviation. The AHP matrix, Table 2.1, is a summary of the rating of each design driver relative to each other as decided by averaging the group members individual AHP matrices. Each design driver (horizontal row) was evaluated against all other design drivers (vertical columns). The range of scores vary from 1/9 to 9 with scores < 1.0 indicating the row criteria is less important than the column criteria and > 1.0 indicating the row criteria is more important than the column criteria.

TABLE 2.1: Analytical Heirarchy Process

Design Drivers		AE	EC	SC	CG	ET	TRL	DC
Aerodynamics Efficiency	AE	1	1	3	3	4	5	6
Empty Fraction	EC	1.00	1	3	3	4	5	6
Stealth Capabilities	SC	0.33	0.33	1	2	3	5	5
CG Margin	CG	0.3	0.33	0.50	1	3	4	4
Ease of Transition	ET	0.25	0.25	0.33	0.33	1	2	3
Technological Readiness Level	TRL	0.20	0.20	0.2	0.25	0.50	1	3
Design Complexity	DC	0.17	0.17	0.2	0.25	0.33	0.33	1
	Sum	3.28	3.28	8.23	9.83	15.83	22.33	28.00

2.1.2 Potential Vehicle Configuration

This section considers a series of 3 types of wing configurations for the design of UCAV as these designs are used extensively for all type of role (Fighter , Attacker , Bomber and Interceptor). Certain configuration are not considered due to lack of ability to work efficiently in both supersonic regime and stealth capability like normal swept back wing .The figure describes the configuration considered .We picked the final configuration of through another round of team discussions, and constructed a second Pugh matrix so as to get a better picture of their relative strengths.

2.1.3 Pugh Matrix

All configurations were compared using a Pugh Matrix [12]. The team scored each config on all of the design drivers on a scale of -5 (least desirable) to +5 (most desirable). These scores were then multiplied by the weights of the design drivers in the normalised priority vector and summed together to get the final individual score for each configuration. The resultant Pugh Matrix and Radar plot of the matrixis shown in table 2.2 and figure 2.1.

TABLE 2.2: Design Driver Evaluation

Design Driver	Weights	Configuration		
		Flying Wing	Blended Wing Body	Variable Sweep Wing
Aerodynamics Efficiency	0.28	2	4	3
Empty Fraction	0.28	2	3	3
Stealth Capabilities	0.16	4	3	2
CG Margin	0.13	0	1	2
Ease of Transition	0.07	-1	1	1
Technological Readiness	0.05	1	2	4
Design Complexity	0.03	-1	1	0
Final Score		1.71	2.77	2.53

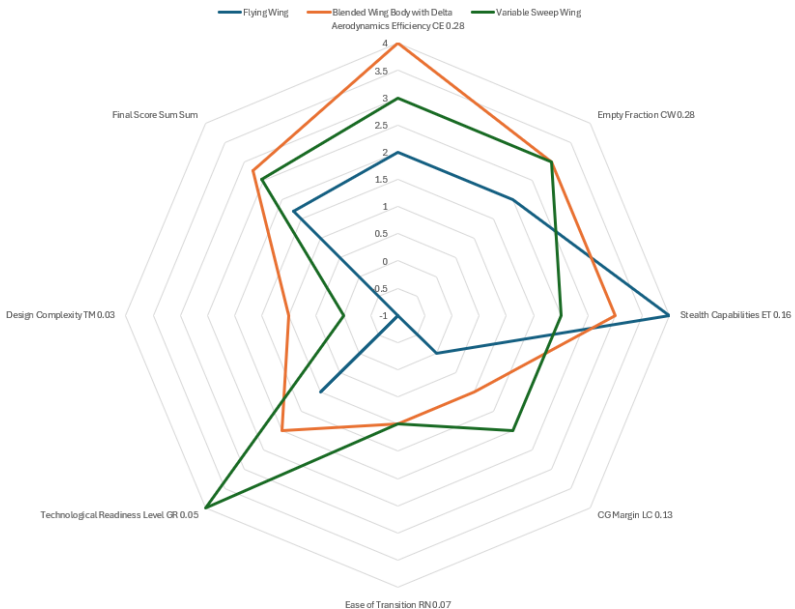


FIGURE 2.1: Radar Plot

2.2 Initial Sizing

2.2.1 Constrain analysis

A constraint analysis was conducted to determine the thrust-to-weight ratio (T/W) versus wing loading (W/S) for a conceptual aircraft design. Multiple performance criteria were evaluated using standard atmospheric models and aerodynamic coefficients at relevant mission phases. The analysis includes ground run requirements during takeoff, rate of climb at sea level, cruise conditions at subsonic (Mach 0.6) and supersonic (Mach 2.3) speeds, and service ceiling capabilities. Using realistic aerodynamic parameters such as drag coefficients (C_D), lift coefficients (C_L), induced drag factor (k), and ground friction coefficient (μ), the required T/W values were plotted against a range of wing loading values from 200 to 6000 N/m². Reference lines were added to the plot for typical fighter and bomber wing loading values, as well as for the maximum allowable angle of climb (AOC). This visual representation helps in identifying feasible design points that satisfy all mission constraints.

Performance Constraints Considered

1. **Take-off Ground Run:** Ensures the aircraft can take off within a specified ground run distance ($S_G = 2000m$).
2. **Rate of Climb:** Maintains a vertical velocity of 55m/s at sea level to meet climb performance requirements.
3. **Subsonic Cruise:** Ensures efficient level flight at Mach 0.6 and an altitude of 1500m.
4. **Supersonic Cruise:** Assesses high-speed cruise capability at Mach 2.3 at an altitude of 14000m.
5. **Service Ceiling:** Ensures the aircraft can maintain a climb gradient at high altitude (defined by a rate-of-climb of 0.508m/s at cruise altitude).
6. **Maximum Angle of Climb (AOC):** Limits are imposed based on a climb angle of 15° and a subsonic lift-to-drag ratio ($L/D_{\text{sub}} = 5$).

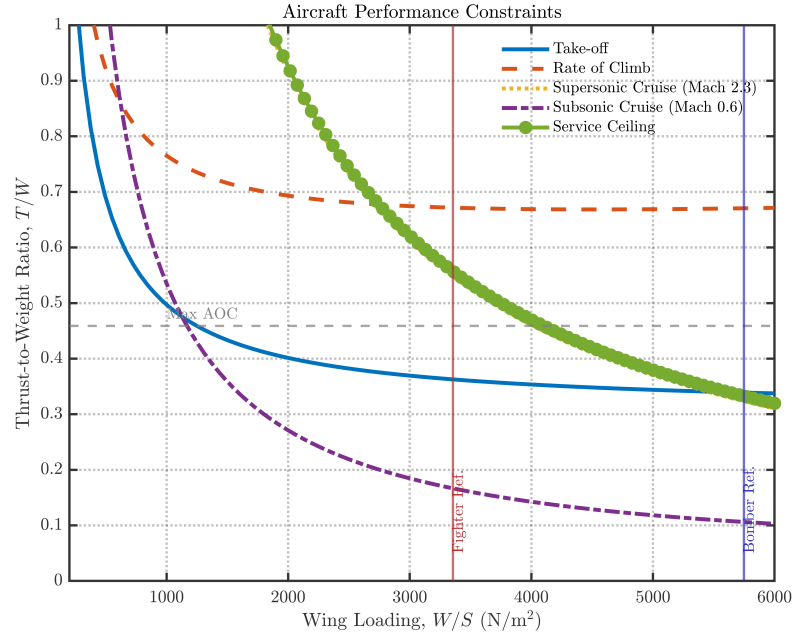


FIGURE 2.2: Constrain Analysis

2.2.2 Weight Estimation

The weight of the aircraft must be designed based on the mission profile and payload requirements. The design takeoff weight W_0 is the total aircraft weight and is composed of:

- Payload Weight: W_{payload}
- Empty Weight: W_e
- Fuel Weight: W_f

Since the UCAV is unmanned, crew weight is not included, and the payload is known. The unknowns are W_e and W_f , and the takeoff weight is given by:

$$W_0 = \frac{W_{\text{payload}}}{1 - \left(\frac{W_e}{W_0}\right) - \left(\frac{W_f}{W_0}\right)} \quad (2.1)$$

2.2.2.1 Empty Weight Estimation

Empty weight (W_e) includes the structure, avionics, propulsion, etc., and can be estimated statistically using empirical trends. For UCAVs, the statistical relation used is:

$$\frac{W_e}{W_0} = 0.65 * 2.392 \cdot W_0^{-0.13} \quad (2.2)$$

2.2.2.2 Fuel Weight Estimation by Mission Segments

Fuel weight is calculated segment-wise using mission weight fractions. For each segment i , the fuel weight burned is:

$$W_{f_i} = \left(1 - \frac{W_i}{W_{i-1}}\right) W_{i-1} \quad (2.3)$$

Weight fractions per segment:

$$\frac{W_1}{W_0} = 0.97 \quad \text{Warm-up and Takeoff} \quad (2.4)$$

$$\frac{W_2}{W_1} = 0.991 - 0.007 \cdot M - 0.010 \cdot M^2 \quad \text{Climb} \quad (2.5)$$

$$\frac{W_3}{W_2} = \exp\left(-\frac{R \cdot C}{V \cdot (L/D)}\right) \quad \text{Cruise} \quad (2.6)$$

$$\frac{W_4}{W_3} = 0.997 \quad \text{Descent (Ingress)} \quad (2.7)$$

$$\frac{W_5}{W_4} = \exp\left(-\frac{E \cdot C}{L/D}\right) \quad \text{Strike (Loiter)} \quad (2.8)$$

$$\frac{W_6}{W_5} = 0.991 - 0.007 \cdot M - 0.010 \cdot M^2 \quad \text{Climb} \quad (2.9)$$

$$\frac{W_7}{W_6} = \exp\left(-\frac{R \cdot C}{V \cdot (L/D)}\right) \quad \text{Return Cruise} \quad (2.10)$$

$$\frac{W_8}{W_7} = 0.995 \quad \text{Descent and Landing} \quad (2.11)$$

2.2.2.3 Total Fuel Weight (with Reserves)

The total mission fuel weight W_{fm} is:

$$W_{fm} = 1.06 \cdot \sum_{i=1}^8 W_{fi} \quad (2.12)$$

2.2.2.4 Iteration for Final Takeoff Weight

Using the calculated empty and fuel weight fractions, a new estimate for W_0 is obtained as:

$$W_0^{\text{new}} = \frac{W_{\text{payload}}}{1 - (1.47 \cdot W_0^{-0.16}) - \left(\frac{W_{fm}}{W_0}\right)} \quad (2.13)$$

This process is repeated iteratively until convergence is achieved.

2.2.2.5 Weight Breakdown

TABLE 2.3: Aircraft Weight Breakdown

Component	Symbol	Weight (kg)
Gross Takeoff Weight	W_0	14 491.5
Empty Weight	W_e	6 484.0
Fuel Weight	W_f	7 007.5
Payload Weight	W_{payload}	1 000.0

TABLE 2.4: Weight Fractions

Fraction	Expression	Value
Empty-to-Gross	W_e/W_0	0.4474
Fuel-to-Gross	W_f/W_0	0.4836
Payload-to-Gross	W_{payload}/W_0	0.0690

2.2.3 Engine Selection

The appropriate propulsion system for an aircraft depends on a number of factors: the design Mach number, altitude, fuel efficiency and cost. From our literature review , its easy to understand that supersonic aircrafts mainly use turbofans and turbojets with

afterburner. There are different types of engines available. Starting from Propeller engines - turboprop, piston prop and turboshaft engines, they have the limitation of producing higher noise and vibration. The propeller by its very nature produces less and less thrust as velocity increases. However, all propeller driven aircraft have a limited cruise Mach number since the propeller tip Mach number cannot exceed approximately 0.7. Then there comes Jet engines which includes Turbofan , Turbojet ,Ramjet and scram jet engines.

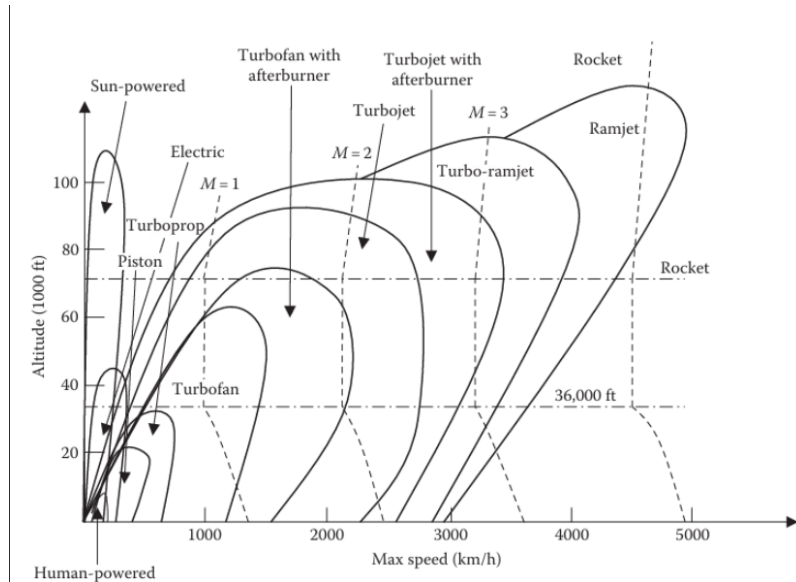


FIGURE 2.3: Powerplant selection

As shown in literature survey, the aircrafts altitude and their mach number are written from the references . when you convert the speed into kmph and altitudes into ft and then match the engine from the below operational envelope , it matches with real-world configurations. Like, the SR-71 with speed of 3540 kmph at an altitude of approximately 80,000ft should use afterburnining turbojets according to the operational envelope and in reality the engine that is used in it was also turbojets with afterburner. Similarly F-22 at 60,000ft with speed 2400 kmph should use turbofan with afterburner and it is used in real. This verification confirms that engine selection based on the operational envelope of altitude versus Mach number is a reliable approach, and it can be confidently applied to select the appropriate engine for our design.

From the above two graphs of figure 2.3 and 2.4 representing Aircraft operational map for Altitude v/s Mach number and specific thrust vs Mach number, the UCAV powerplant suitable for the mission is:

- Low Bypass Ratio Turbofan

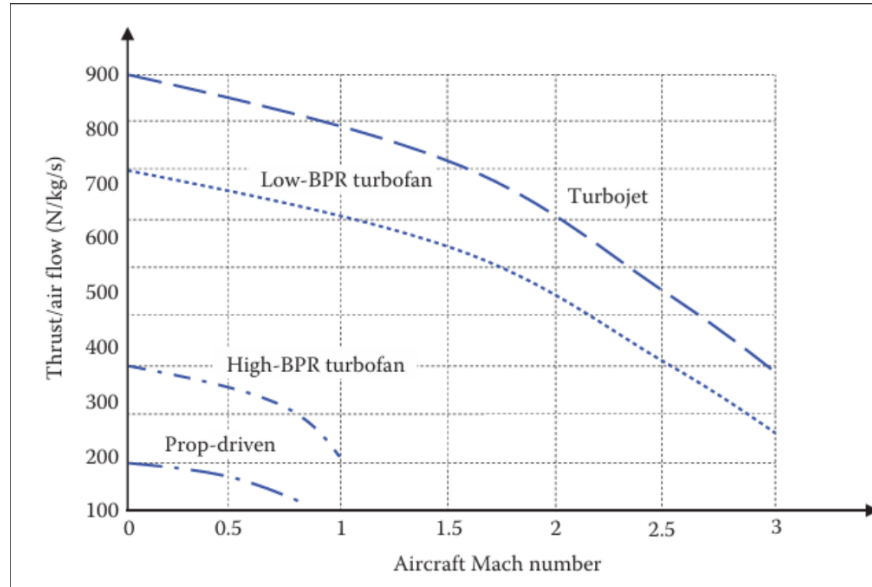


FIGURE 2.4: Thrust vs mach number

- Turbojets with Afterburner

The turbofan engine offers better efficiency than a turbojet at subsonic speeds, but at supersonic and higher speeds the drag of the fan increases so that the net benefit reduces. Aircraft designed for efficient operation at speeds over Mach 2 are likely to have pure turbojets. Turbojets have higher exit velocity than turbofans. Also , turbofans have large frontal area due to which it has high chances of encountering wave drag at supersonic speeds. The absence of bypass reduces the chance of managing bypass air flow. So we selected turbojets. Afterburner becomes inefficient in terms of fuel usage. The fuel flow required to produce a pound of thrust in afterburner is approximately double that used to produce a pound of thrust during normal engine operations. Here afterburner will be used while take-off or climb to achieve the required cruise altitude.

2.2.4 Airfoil Selection

These airfoils refer to airfoils designed for flight above Mach 1. They are thin airfoils ($t/c = 0.03\text{--}0.065$) with sharp leading edges. They also include diamond-shaped airfoils (ideal for theoretical analyses) and biconvex airfoils (used in limited aircraft, including the *F-104 Starfighter*) [13]. There exist NACA supersonic airfoils named NACA 64A003 ($t/c = 3\%$), NACA 64A004 ($t/c = 4\%$), NACA 64A005 ($t/c = 5\%$), and NACA 64A006 ($t/c = 6\%$). For the current analysis, these airfoils can be used for the wing, considering

aerodynamic, stability, and structural characteristics. As NACA 64A003 is very thin, we eliminate this airfoil due to its thickness. The other three airfoils will be used for our study. These airfoils will be optimized in our future studies based on the algorithm discussed in the following section.

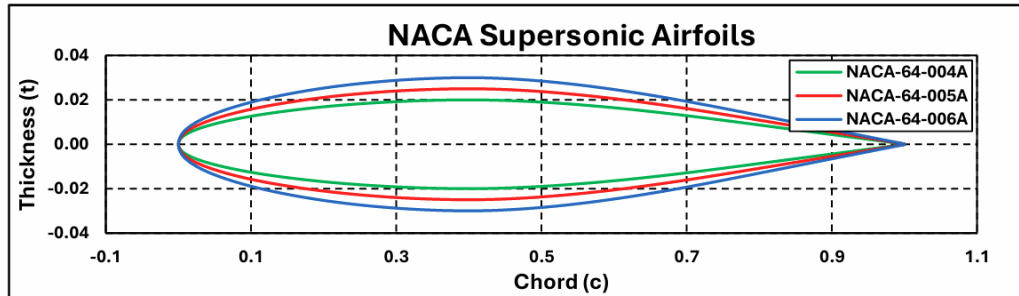


FIGURE 2.5: Supersonic airfoil comparision

TABLE 2.5: NACA 64A Series Airfoil Characteristics

Airfoil	Characteristics			
	Thickness (%)	Thickness Loc. (%)	Camber (%)	Camber Loc. (%)
NACA 64A004	4	39.74	0	0
NACA 64A005	5	39.74	0	0
NACA 64A006	6	39.74	0	0

2.3 Multidisciplinary Design Analysis and Optimization

The Figure 2.6 below is the algorithm used to get the parameters of the wing. First, we decide our design variables, such as Mach number, Reference Area, TE Sweep, Twist, Dihedral, Aspect Ratio, and Taper Ratio. We have added the Mach number as the design variable because the minimum Mach number is 1.85 based on the mission requirements, but the maximum Mach number can vary. We have tried to use non-dimensional parameters, such as Aspect Ratio and Taper Ratio, instead of directly selecting span, root chord, and tip chord to make our design algorithm simpler. Once the design variables are, they are fed into the OpenVSP tool using OpenVSP APIs, which will generate the wing shape. From here, a 3D plot file is generated and fed to the flight software. We apply all the boundary conditions, and reference values and aerodynamic loads are generated for the given Mach number. Once the aerodynamic loads are generated, we calculate the cruise CL, CD, Drag,

Thrust, and based on these values, we calculate our take-off weight and iterate it with the help of formulas provided by Raymar, which are explained in the further section. This final weight is used to calculate the final L/D because, with a change in weight as it is iterated, the cruise L/D also changes. Once the weight and L/D converge, the flight score is calculated. This is our objective function, which needs to be maximized. The flight score is fed into the optimizer, which will decide the new value of the design variables based on the slope. The slope is calculated with the help of finite differences, as there is a black box (and not some analytical function) between the design variables and the objective function. Gradient descent will give the local minimum or maximum value. To find the global maximum value, we have used Latin Hypercube sampling to cover the whole design space. The upper and lower bounds of the design variables are decided using market data, mission objective, past experience.

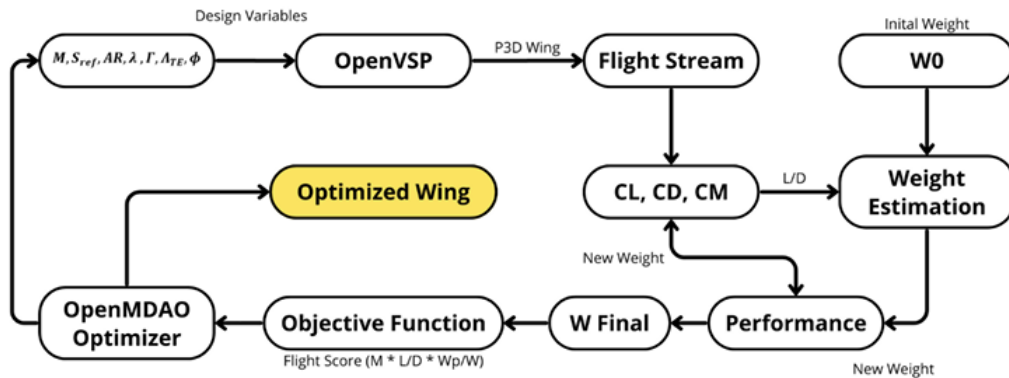


FIGURE 2.6: Wing design MDAO algorithm

2.4 Final Design

2.4.1 Wing

The wing design is done using the algorithm explained in the design methodology section. This is the final wing obtained from the gradient descent code. Below are the wing parameters.

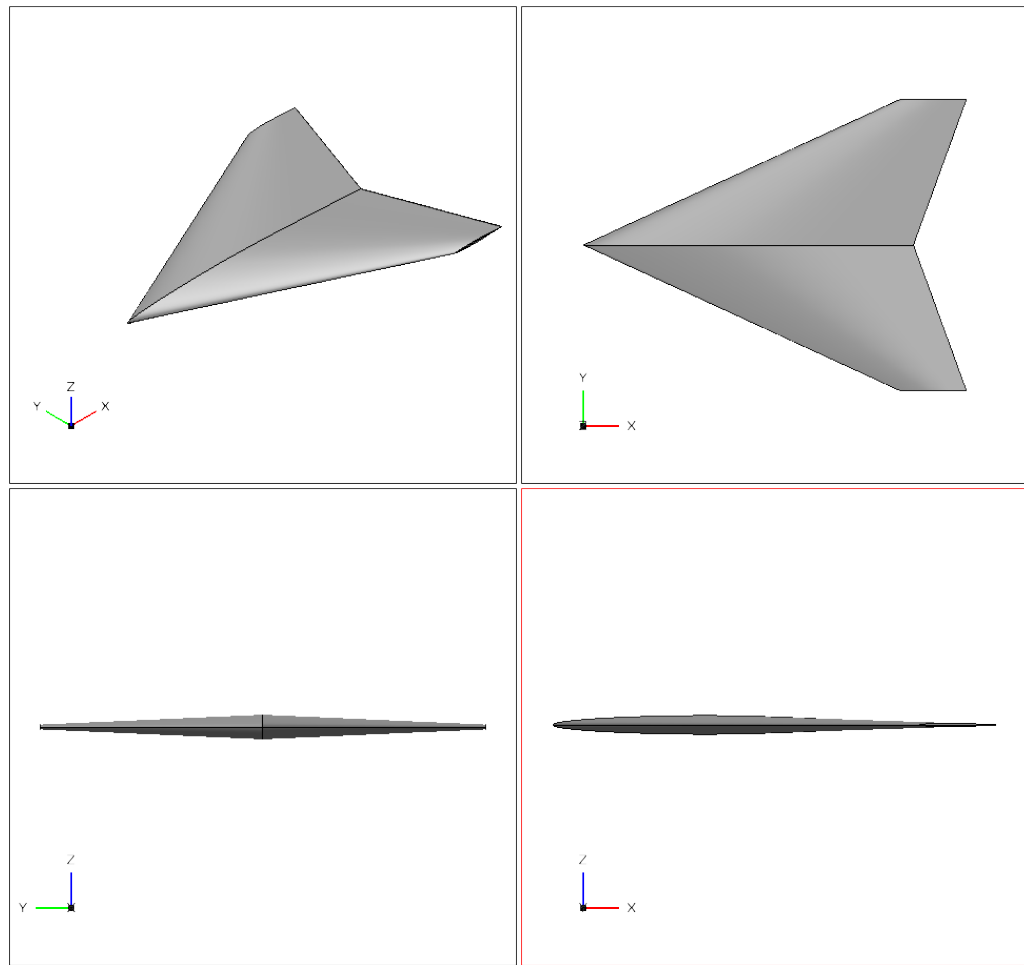


FIGURE 2.7: Final wing 3 view

TABLE 2.6: Wing Parameters

Wing Parameter	Symbol	Value	Unit
Reference Area	S_{ref}	33.4	m^2
Total Span	b	7	m
Mean Aerodynamic Chord	c_{mac}	5.44	m
Root Chord	c_{root}	7.9	m
Tip Chord	c_{tip}	1.58	m
TE Sweep	Λ_{TE}	20	degrees
Twist	ϕ	0	degrees
Dihedral	Γ	0	degrees
Aspect Ratio	AR	1.5	—
Taper Ratio	λ	0.2	—

2.4.2 Payload Bay

For the current mission, there are three kinds of payload configurations:

- **Strategic Ground Attack:** Contains a total of 4 guided bombs.
- **Air Combat:** Contains 4 air-to-air missiles and 1 anti-radiation pod.
- **Electronic Warfare:** Contains 1 anti-radiation pod and 2 guided bombs.

The dimensions of each payload type are listed in Table 2.7.

TABLE 2.7: Payload Dimensions

Payload Type	Diameter (mm)	Length (mm)
Guided Bomb	250	2500
Air-to-Air Missile	125	3000
Anti-Radiation Pod	300	5500

To accommodate structural components such as fins, pylons, avionics, launch mechanisms, and electrical harnessing, a clearance factor of 1.2 times the payload diameter is considered in all dimensions.

Based on these considerations, the final dimensions of the payload bay are given in Table 2.8.

TABLE 2.8: Payload Bay Dimensions

Dimension	Value	Unit
Length	5.775	m
Width	1.2	m
Height	0.36	m

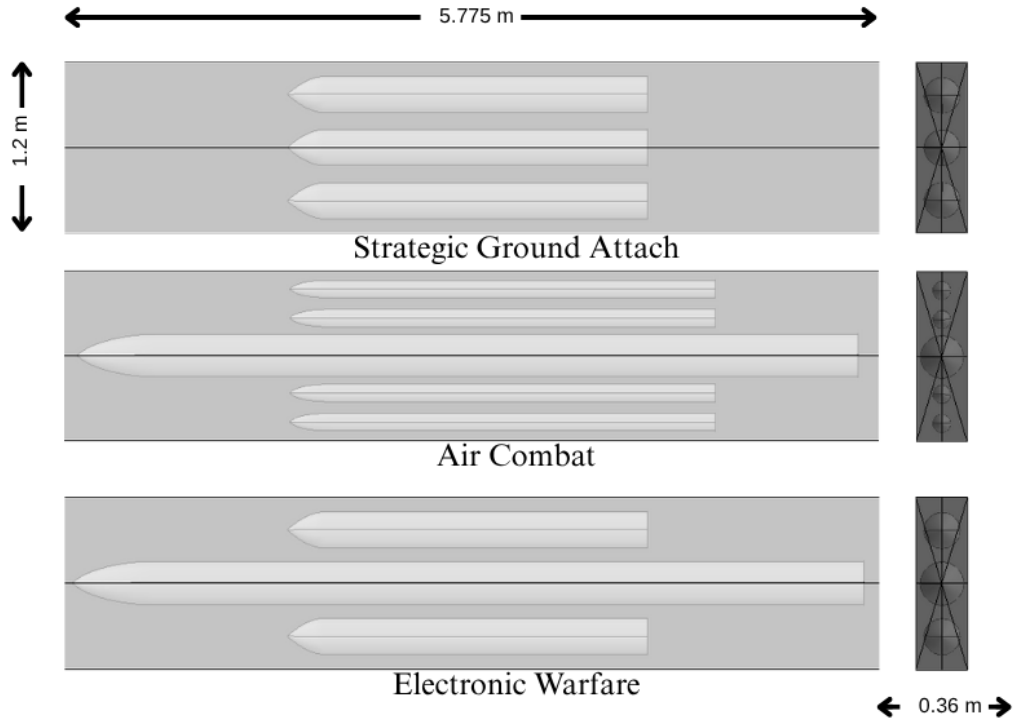


FIGURE 2.8: Payload Bay Configuration in OpenVSP

As shown in Figure 2.8, the payload bay configuration is modeled in OpenVSP. All payload components—guided bombs, air-to-air missiles, and the anti-radiation pod—are created based on the specified dimensions. Proper clearance ($1.2 \times \text{Dia}$ of pod) has been maintained for fins, pylons, structural supports, avionics, launch mechanisms, and electrical harnessing.

2.4.3 Fuselage

The fuselage sizing has been primarily focused on blending the wing with the fuselage body while accommodating the full payload bay internally. Since the payload bay is designed as a single, integrated unit, it is positioned at the bottom of the fuselage. This downward placement causes the lower fuselage to appear bulky, as shown in Figure 2.9, which may contribute to increased drag.

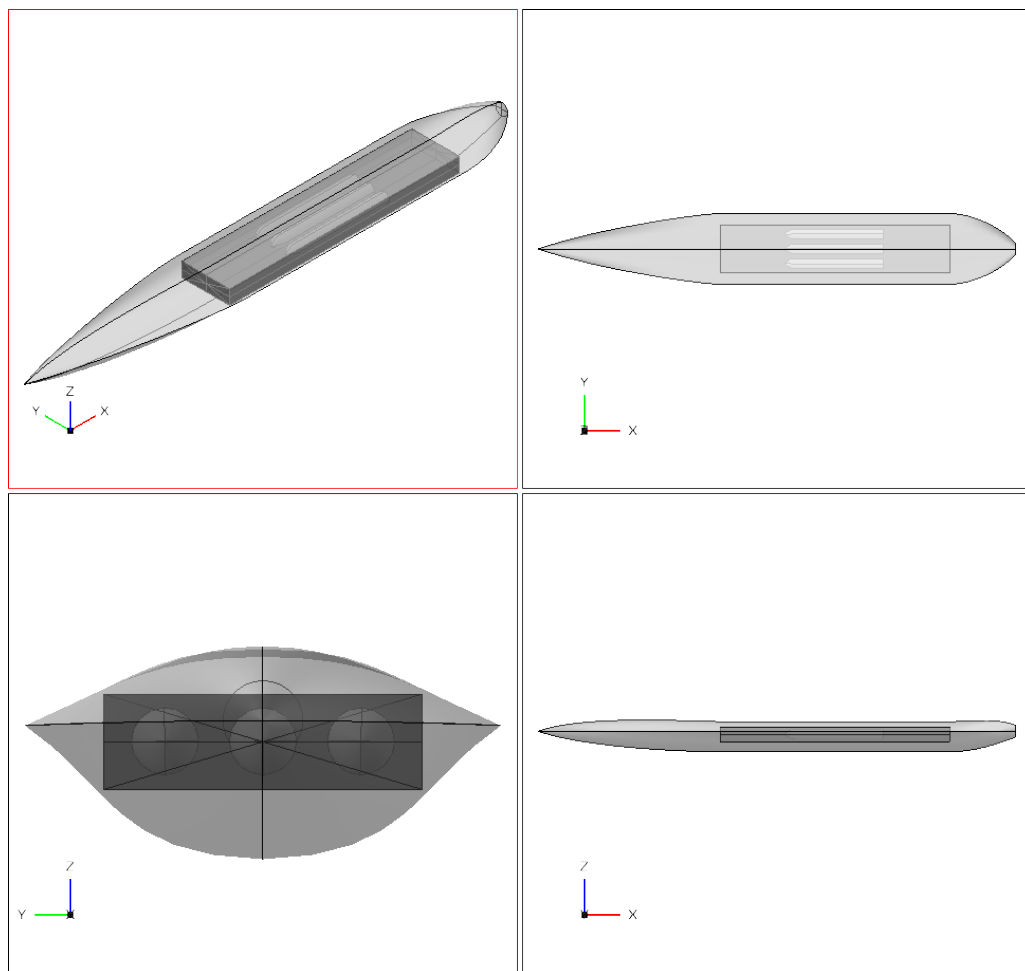


FIGURE 2.9: Fuselage and Payload Bay Integration in OpenVSP

2.4.4 Final Design

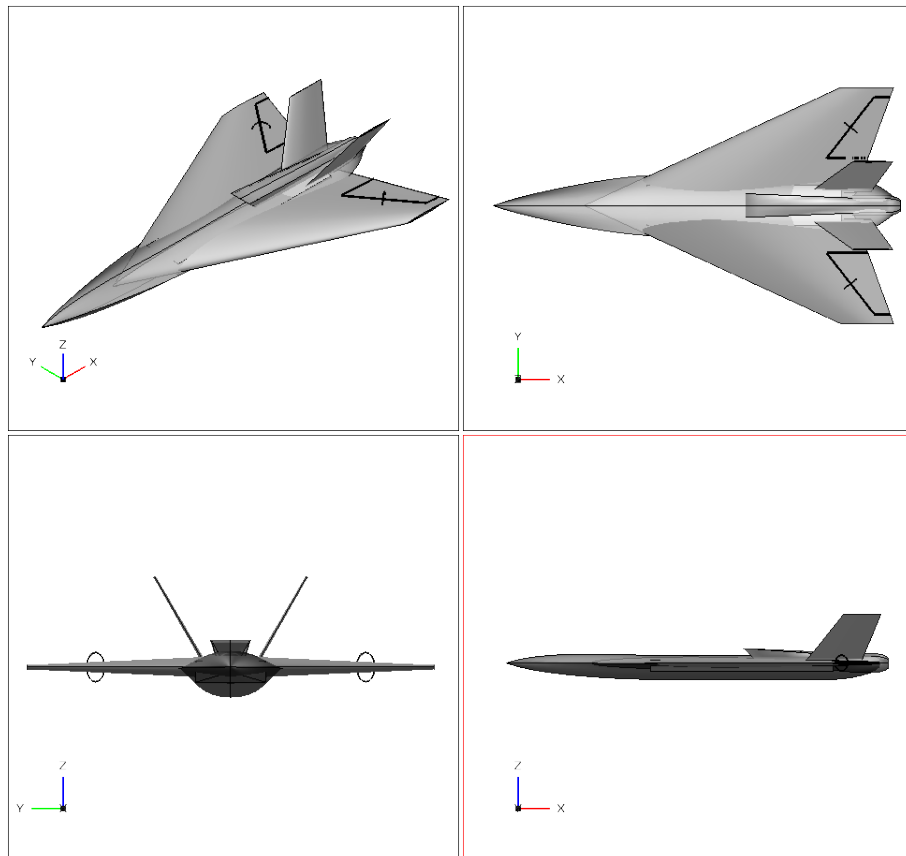


FIGURE 2.10: Final Design in OpenVSP

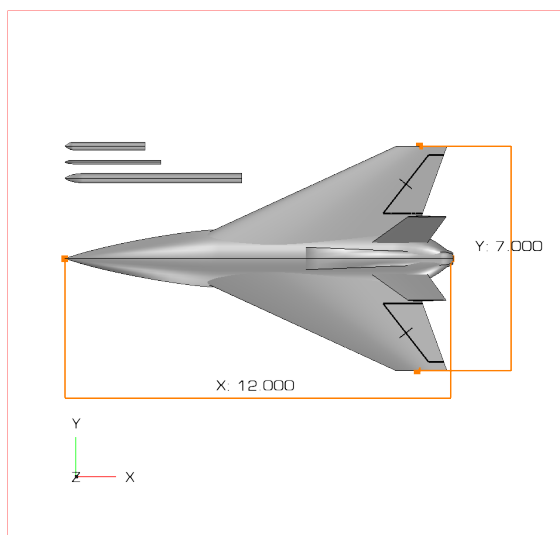


FIGURE 2.11: Figure: Basic Dimensions

Figures 2.10 and 2.11 illustrate the final configuration of the aircraft. The detailed wing design parameters are provided in Table 2.6. These figures also highlight the relative size of the payload compared to the overall dimensions of the aircraft.

2.4.5 Engine Inlet

Turbojet engine can operate much efficiently if air entering them is slowed to a speed of about Mach 0.4-0.5 . The type and geometry of the inlet and inlet duct will determine the pressure loss and distortion of the air supplied to the engine, which will affect the installed thrust and fuel consumption. Also, the inlet's external geometry including the cowl and boundary-layer diverter will influence the aircraft drag. Currently for the design of UCAV uses the 2-D ramp inlet (External compression inlet system), the reason being the sum of the losses through the oblique and the final normal shock will be less than the huge loss through a single normal shock . The speed reduction and pressure recovery through an oblique shock depends upon the angle of the wedge or cone used to establish the shock.

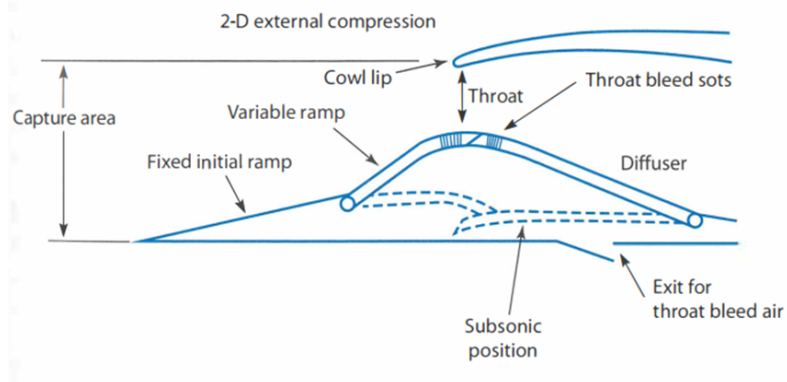


FIGURE 2.12: Variable Inlet Geometry

Approaching the cruise mach number of Mach 2.3 it would be ideal to use variable inlet geometry and keep the initial ramp angle at 15 degrees leading to efficient pressure recovery during the different regimes of the UCAV . A rule of thumb is used for inlet selection criteria as given in figure

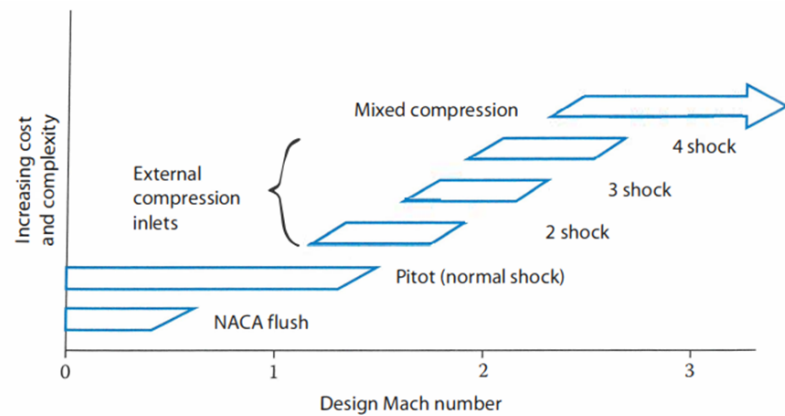


FIGURE 2.13: Inlet Selection Criteria

The location of inlet since it is unmanned would be ideal at the top of the fuselage making the streamlined air from fuselage directly to inlet only disadvantage the upper fuselage inlet is poor at high angle of attack because the forebody blanks the airflow .



FIGURE 2.14: Upper Fuselage Inlet

Chapter 3

Aerodynamic Analysis

The aerodynamic analysis is carried out using Flight Stream software. The atmospheric conditions correspond to the Indian Reference Atmosphere at an altitude of 14 km. The parameters used for the simulation are listed in Table 3.1.

TABLE 3.1: Atmospheric data at 14 km Altitude

Parameter	Symbol	Value	Unit
Pressure	P	13986.86	Pa
Temperature	T	227.94	K
Density	ρ	0.2138	kg/m ³
Speed of Sound	a	302.63	m/s
Dynamic Viscosity	μ	1.482862×10^{-5}	Pa·s
Gas Constant	R	287	J/kg·K
Ratio of Specific Heats	γ	1.4	—

The aerodynamic analysis includes both subsonic and supersonic flight regimes. In the supersonic regime, the low-order (steady) flow model does not account for stall prediction. However, in the subsonic regime, stall is observed at approximately 20 degrees angle of attack. Another critical aerodynamic aspect is the pitching moment coefficient. From the analysis, it is observed that the aircraft's stability improves due to the aft shift of the aerodynamic center. This shift results in a slight change in the slope of the pitching moment curve when comparing the subsonic and supersonic regions. Thus the change in static margin is very less.

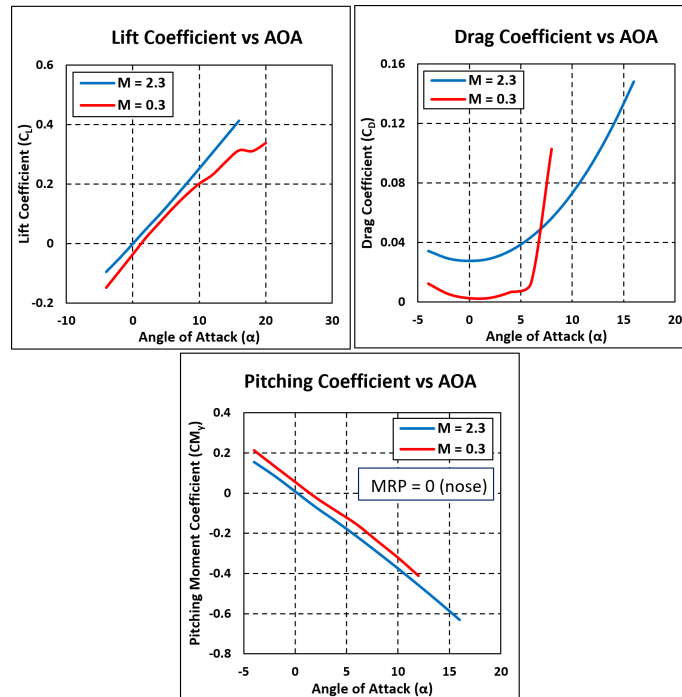


FIGURE 3.1: Aerodynamic data (Alpha Sweep) for subsonic and supersonic

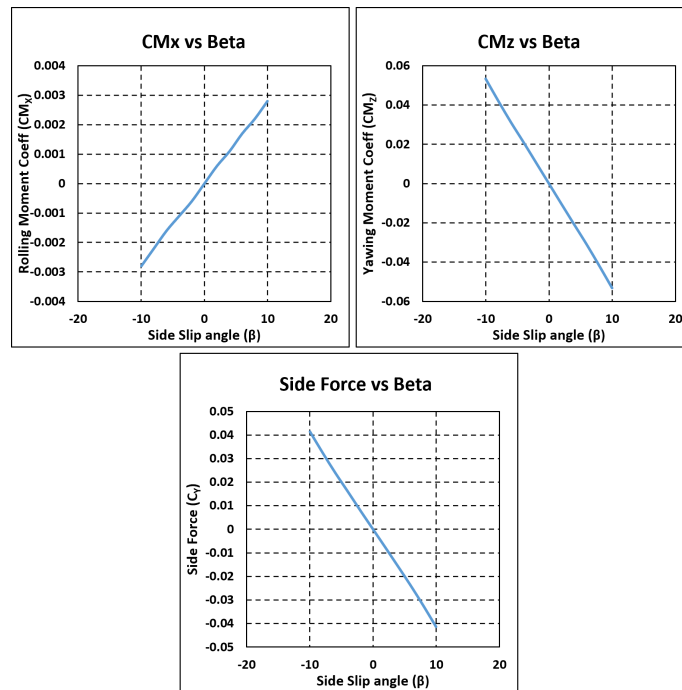


FIGURE 3.2: Aerodynamic data (Beta Sweep) for supersonic

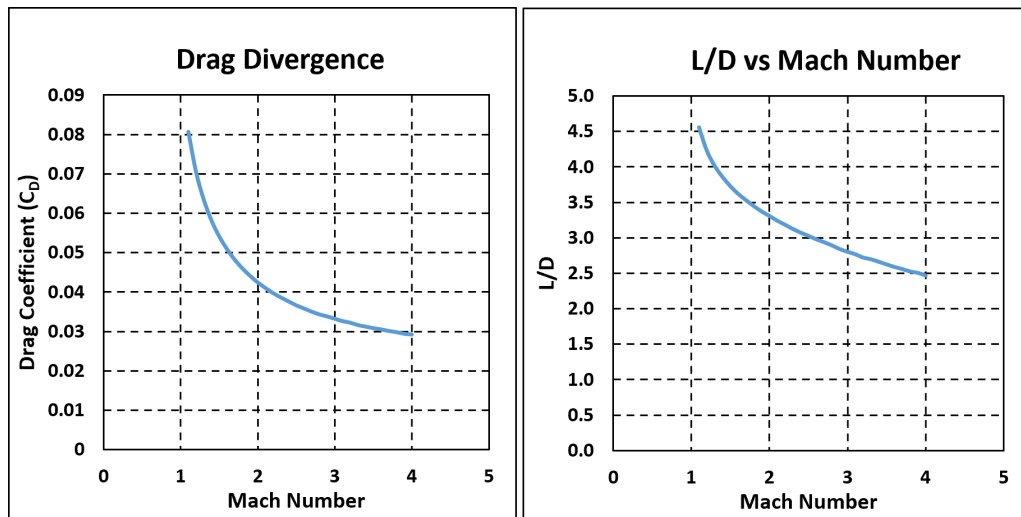


FIGURE 3.3: Drag Divergence and L/D vs Mach number

The drag characteristics clearly show that drag is significantly higher in the supersonic regime compared to the subsonic regime, as evident from the drag divergence graph.

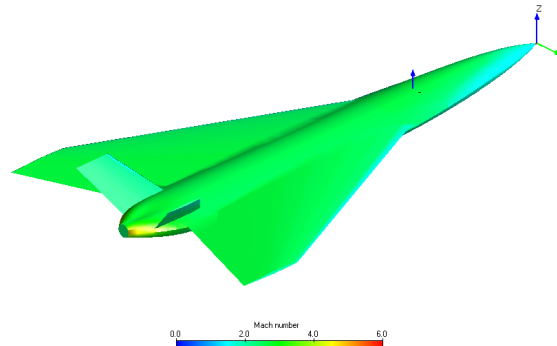


FIGURE 3.4: Mach Contour

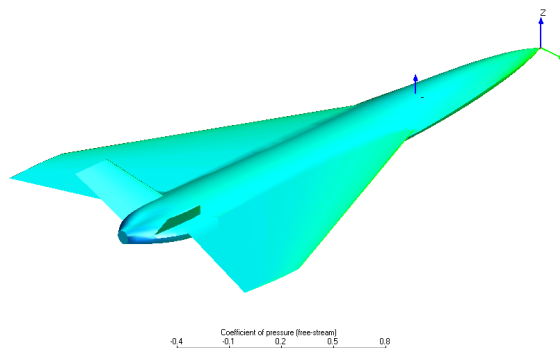


FIGURE 3.5: Pressure Contour

Chapter 4

Performance and Stability Analysis

4.1 Background

The efficacy of a design is assessed through a thorough performance analysis process. The purpose of this procedure is to determine the design's capability to manage the situations that it is likely to encounter during its mission. The outcome of this evaluation is an assurance of the reliability of the performance of the operator.

Another equally important aspect of design evaluation to consider concerns the stability of the aircraft. A stable aircraft exhibits the ability to maintain steady flight and, in case of disturbances, to return to its steady state. This directly contributes to the safety of the aircraft.

Together, these analyses guide design trade-offs. They enable designers to strike an optimal balance between competing performance requirements while ensuring flight safety in the operational envelope.

4.2 Performance Evaluation

4.2.1 Range Evaluation

The range is defined as the maximum distance that an aircraft can travel during steady, level flight without refueling. This distance is influenced by a variety of design and operational factors, including aircraft weight, engine efficiency, aerodynamic performance, and atmospheric conditions. For flights at a constant speed, the range can differ significantly depending on the altitude. Also, when flying at a constant altitude, the range will vary with changes in flight speed due to changes in the L/D ratio and fuel consumption rates. This subsection explores how the range of aircraft is affected by both these factors. This provides a comparative analysis to highlight the conditions under which maximum range can be achieved.

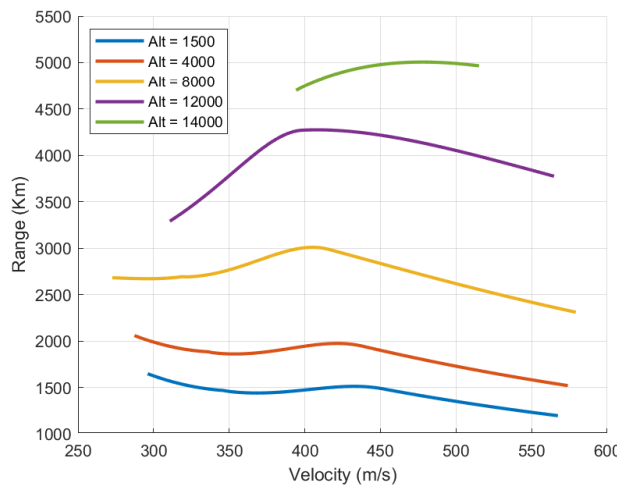


FIGURE 4.1: Range vs Speed at Various Altitudes

It is observed in figure 4.1 that at lower altitudes maximum range is achieved at subsonic speeds while at higher altitudes, this happens at supersonic speeds. The ground speed of the aircraft also increases at these altitudes.

4.2.2 Level Turn

Level turning performance ensures mission flexibility and survivability during high-speed operations. A level turn allows the UCAV to change its heading while maintaining constant altitude, which is vital during evasive maneuvers or precise target approach in a contested airspace. This section shows two key aspects of turning performance: instantaneous turn

and sustained turn. The instantaneous turn reflects the maximum achievable turn rate at a given moment and is limited by structural or aerodynamic constraints. It is critical for quick maneuvers during combat engagement or threat evasion. The sustained turn, on the other hand, represents the ability of the UCAV to maintain a constant turn rate over time, without losing speed or altitude. These metrics aid in rating the agility of the aircraft and are provided in the figure 4.2 & 4.3.

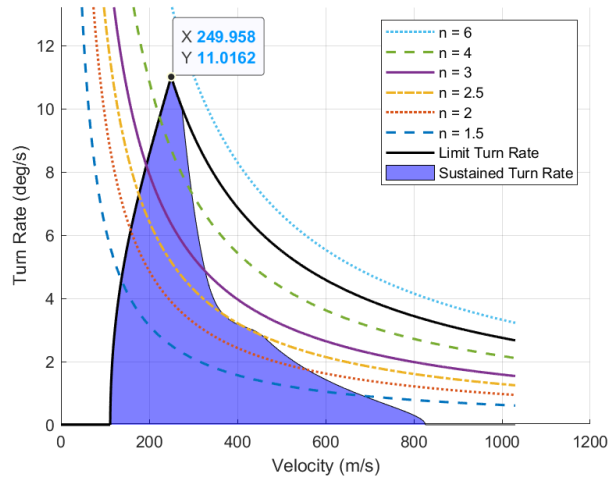


FIGURE 4.2: Turn Characteristics During Loiter

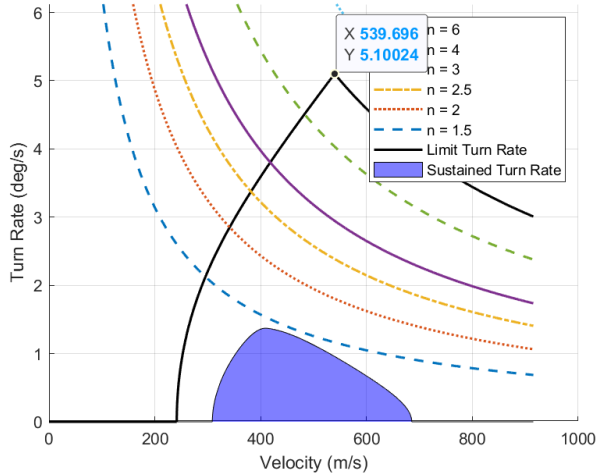


FIGURE 4.3: Turn Characteristics During Cruise

4.2.3 Gliding Flight

Gliding flight is a critical aspect of an aircraft's performance evaluation. The subsection focuses particularly on scenarios involving engine failure or power-off descent. For a supersonic UCAV bomber, understanding gliding behavior is essential for assessing its ability to safely reach a recovery zone or minimize radar exposure during silent approach. In gliding flight, the aircraft descends at a steady rate without engine thrust, relying solely on its aerodynamic forces. Two key parameters that characterize this flight mode are the glide angle, which determines how far the aircraft can travel horizontally for a given loss in altitude, and the sink rate, which indicates the vertical speed of descent. These metrics are influenced by the lift-to-drag ratio and Velocity.

The glide angle is given as the ratio of Drag to Lift. The minimum sink rate is given as the component of velocity in direction of glide angle :

$$\tan(\gamma) = \frac{C_d}{C_l}$$

$$V_v = V \cdot \sin(\gamma)$$

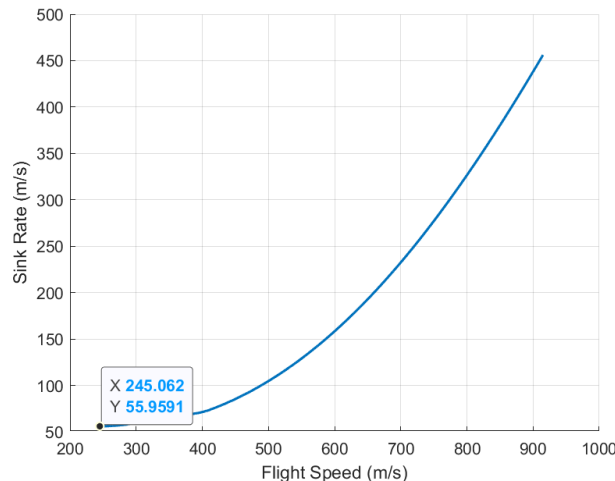


FIGURE 4.4: Sink Rate with Speed (Cruise) at 100% Weight

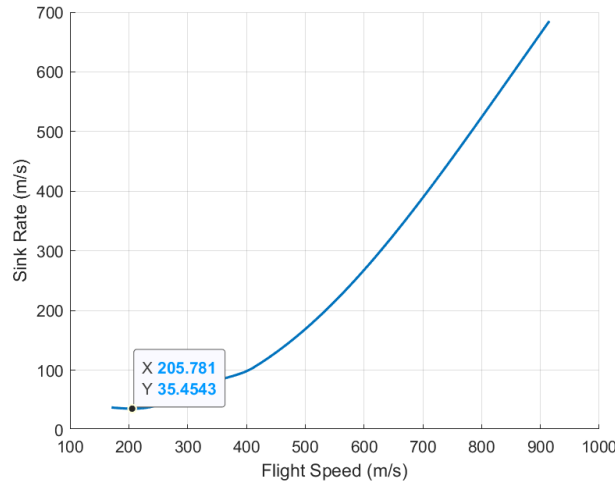


FIGURE 4.5: Sink Rate with Speed (Cruise) at 50% Weight

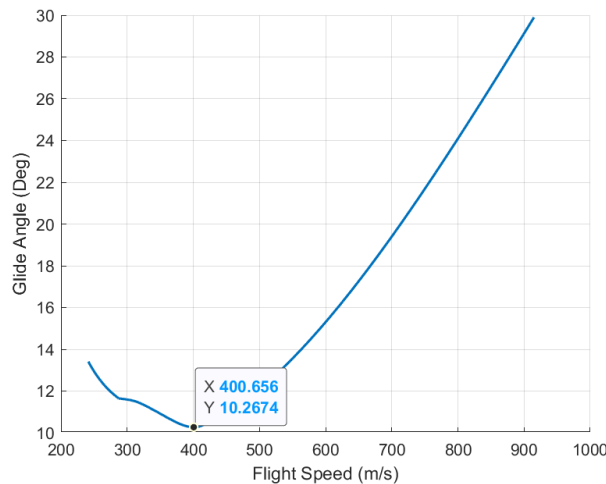


FIGURE 4.6: Glide Angle with Speed (Cruise) at 100% Weight

4.2.4 Thrust - Drag Comparison at Specific Altitudes

A direct comparison between thrust available and aerodynamic drag gives a margin of the aircraft during steady flight. This comparison is carried out at cruise altitude and loiter altitudes. Thrust available is governed by the engine's capability, which varies with altitude and Mach number. Drag force depends on the aircraft's shape and also changes with altitude and Mach number. By plotting and analyzing these two parameters, this section identifies the flight regimes where the UCAV can maintain level flight, accelerate, or decelerate.

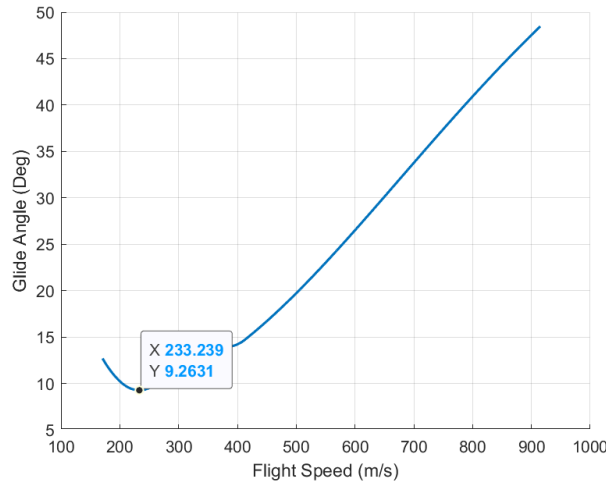


FIGURE 4.7: Glide Angle with Speed (Cruise) at 50% Weight

Note: An error was made while selecting the engine, as the effect of air density at cruise on thrust was not counted. This has left an underpowered engine. This has led to aircraft not meeting thrust requirements.

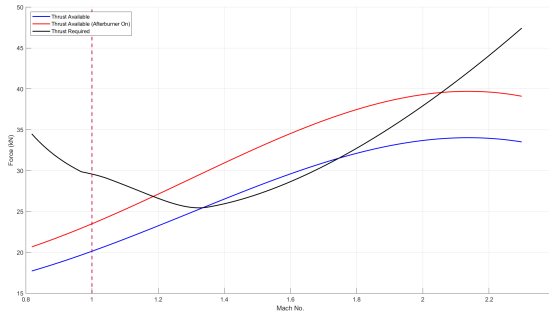


FIGURE 4.8: Thrust Profile at Cruise Altitude

4.2.5 Energy Maneuverability Methods

The Energy Maneuverability methods are analytical tools to evaluate the combat performance and agility of an aircraft by examining its energy state and energy rate capabilities. Originally developed for fighter aircraft, these tools are valuable for a supersonic UCAV bomber too. This is because in addition to operating in high-threat environments energy management can be critical for mission success. This method considers the aircraft's total specific energy—comprising both kinetic and potential energy—and how rapidly it can gain or lose that energy under different flight conditions. By analyzing Height Energy

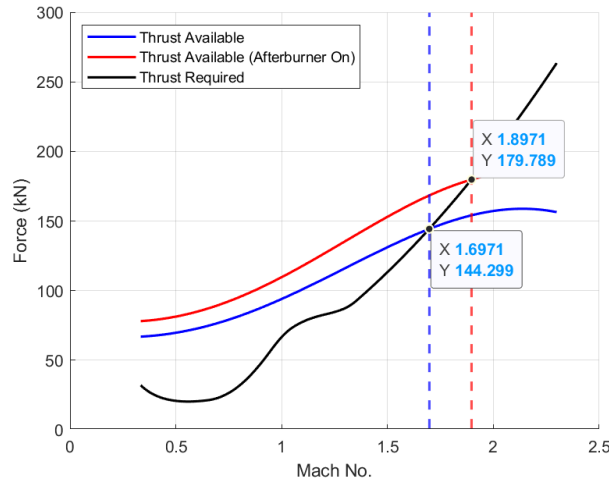


FIGURE 4.9: Thrust Profile at Loiter Altitude

(He) contours and specific excess power (P_s) across a range of altitudes and velocities, the EM approach provides a clear visualization of where the aircraft can accelerate, climb, or sustain turns effectively.

$$H_e = \frac{E}{W} = h + \frac{1}{2g} * V^2$$

$$P_s = \left(\frac{T - D}{W} \right) \cdot V$$

Specific Excess Power (P_s) is a key performance metric that represents the aircraft's ability to accelerate, climb, or maneuver at a given flight condition. It is defined as the rate of change of specific energy (sum of potential and kinetic energy) per unit mass, provides a direct measure of the energy available for tactical maneuvers.

It is given as:

$$P_s = \left(\frac{T - D}{W} \right) \cdot V$$

The drag force can be further expanded to give

$$P_s = V \left[\left(\frac{T}{W} \right) - \frac{q \cdot C_{D0}}{W/S} - n^2 \cdot \left(\frac{K}{q} \right) \cdot \left(\frac{W}{S} \right) \right]$$

The Specific Excess Power can be understood to be dependent on 4 Factors:

- Thrust Force
- Drag Force
- Weight of Aircraft
- Flight Speed

These factors are a function of 3 independent variables. These variables are:

- Mach No.
- Altitude
- Load Factor

This means that the complete performance envelope of the aircraft can be generated by varying these variables and the specific excess power.

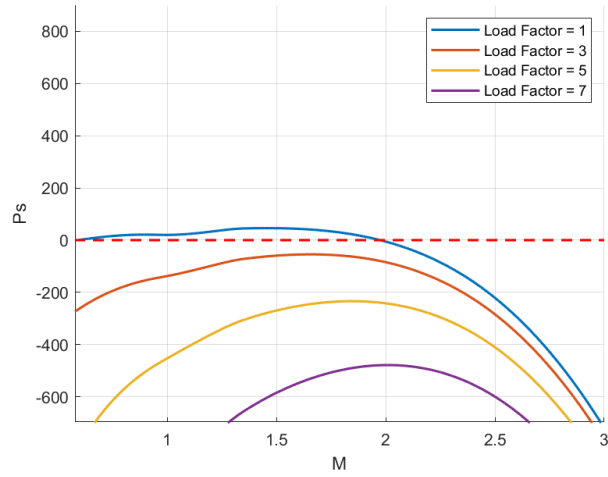
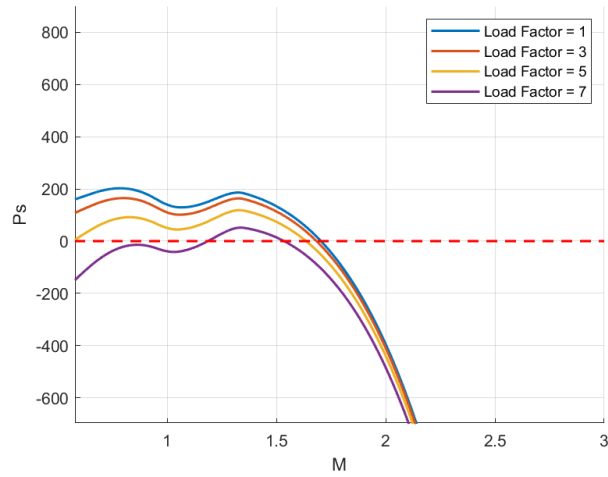
4.2.5.1 P_s vs M

The P_s variation with Mach No. at a set of load factors for a given altitude is shown in figure 4.10 and 4.11.

Note: An error was made while selecting the engine, as the effect of air density at cruise on thrust was not counted. This has left an underpowered engine. This has led to aircraft not meeting thrust requirements.

4.2.5.2 Alt vs M

The Altitude vs Mach no. graph gives a limit of performance. The maximum achievable Mach is also shown to be 2.300.

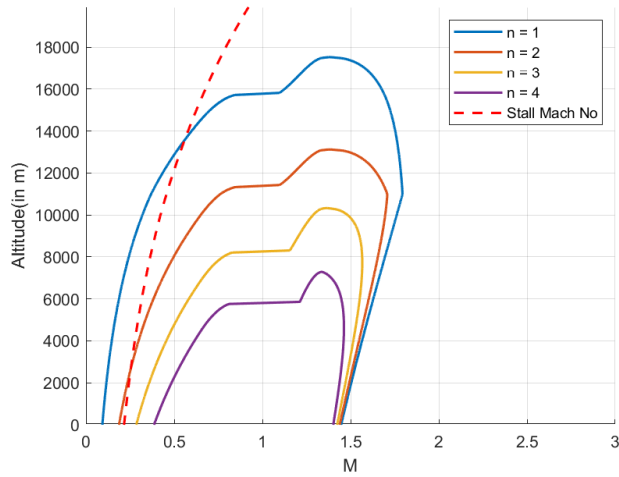
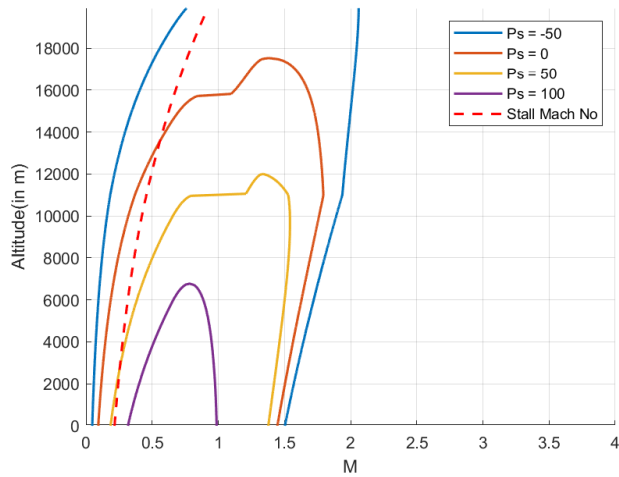
FIGURE 4.10: P_s vs M at Cruise AltitudeFIGURE 4.11: P_s vs M at Loiter Altitude

4.2.5.3 P_s vs Ψ

The level turn rate is dependent on the load factor and thus can be plotted with respect to P_s at input Altitude and Mach no.

4.2.6 Minimum Time To Climb

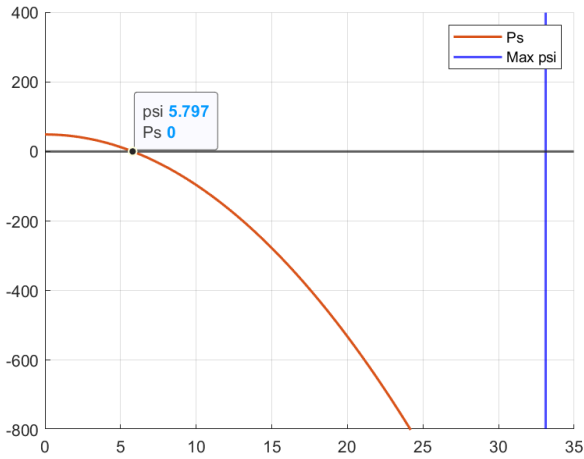
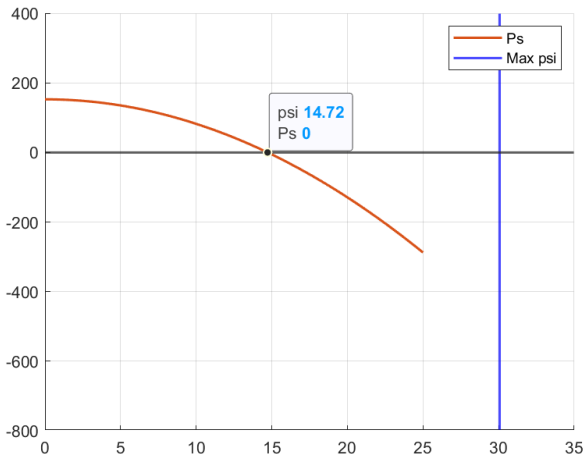
A distinctive requirement of this design is the need to minimize the aircraft's time to climb. Given the mission's strict time constraints, it is critical that all phases of flight,

FIGURE 4.12: Alt vs M, $Ps=0$ FIGURE 4.13: Alt vs M, $n=1$

including climb, are completed in the shortest possible time. Consequently, the aircraft's climb performance must be capable of meeting these time-sensitive operational demands.

The minimum time to climb is the time taken by the aircraft to reach from an input initial mach number and altitude to a final mach number and altitude within the stipulated time frame.

The time to climb can be estimated ratio of height energy change to the specific excess power.

FIGURE 4.14: Ps vs Ψ , $M = 0.9$, $Alt = 9000m$ FIGURE 4.15: Ps vs Ψ , $M = 0.5$, $Alt = 1500m$

$$t_{1-2} = \frac{\Delta H_e}{P_s}$$

A simulation is conducted where the aircraft first reaches the best climbing mach no and height energy at its altitude. Then it starts climbing in a manner so that for a set change in height energy, the maximum average Ps value is present. If aircraft reaches required height energy before reaching required altitude, it will follow a trajectory of constant height energy. This happens by reducing speed and converting the kinetic energy into the potential energy. If the aircraft reaches the required altitude first, it will directly increase

it's mach no to reach final state. In the simulation, the aircraft initially accelerates and climbs to achieve the best climbing Mach number and corresponding height energy for its current altitude. This point marks the beginning of the climb phase. From this point onward, the aircraft ascends in a manner designed to maximize the average specific excess power (P_s) over each incremental change in height energy. This approach ensures the climb remains as efficient as possible within the energy-performance envelope of the design.

If the aircraft attains the required height energy before reaching the target altitude, it follows a trajectory that maintains constant height energy. The aircraft reduces its speed, converting kinetic energy into altitude.

Conversely, if the aircraft reaches the desired altitude before achieving the required final height energy, it increases its Mach number at constant altitude to reach the final energy state.

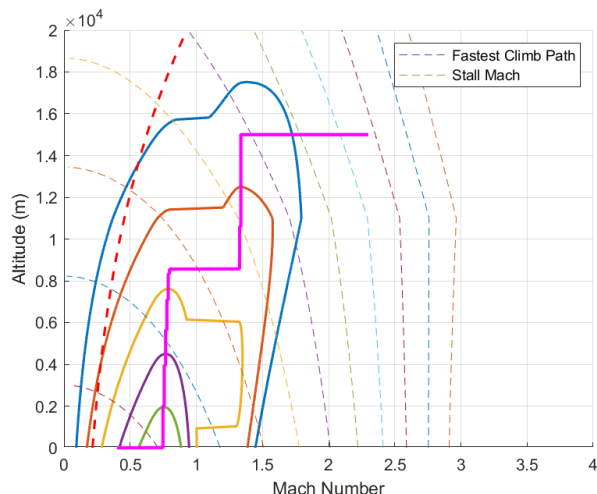


FIGURE 4.16: Climb Path from Takeoff to Cruise

The aircraft requires a minimum of 207.22 seconds to reach the cruise condition from the takeoff condition.

The aircraft requires a minimum of 199.78 seconds to reach the cruise condition from the takeoff condition.

4.2.7 Takeoff Performance

The takeoff and landing analysis follows the estimation techniques presented in [refer [5] and [4]]. This subsection estimates the minimum runway length and thrust requirements

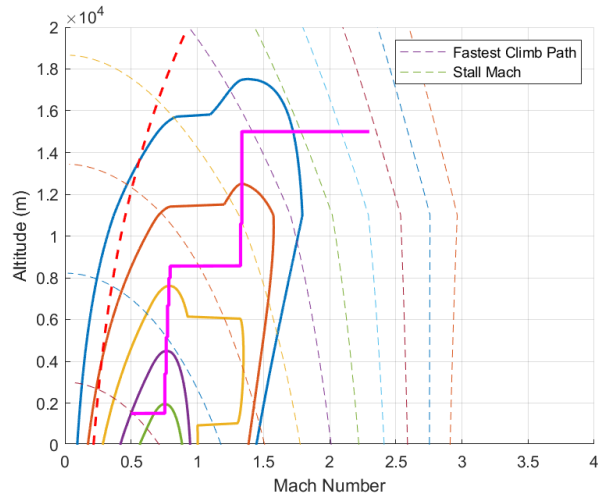


FIGURE 4.17: Climb from Loiter to Cruise

needed for a safe takeoff. Precise takeoff analysis ensures mission readiness from varied airfields.

The takeoff sequence is analyzed in four primary phases:

- Ground Roll: The distance required for acceleration from rest to rotation speed was calculated to be 1344.90 meters.
- Rotation Roll: The distance during the pitch-up maneuver before lift-off is 230.77 meters.
- Transition Roll: The curved climb-out trajectory immediately after lift-off, computed as 280.97 meters.
- Climb Roll: The final segment required to reach the defined obstacle clearance height, totaling 33.40 meters.

Based on these components, the total takeoff length is estimated at 1849.10 meters

4.2.8 Landing Performance

To assist with deceleration, the aircraft is equipped with a drogue parachute, enhancing braking effectiveness and reducing ground roll distance. The landing sequence is evaluated through the following distinct phases:

- Approach Segment: Distance covered during the final steady descent toward the runway — 290.79 meters.
- Flare Segment: The nose-up maneuver executed to reduce descent rate before touch-down — 284.97 meters
- Rotation Segment: The brief nose pitch-down following touchdown — 230.77 meters
- Ground Roll: Distance required to bring the aircraft to a full stop, including braking and drag deceleration — 820.55 meters

The total estimated landing length is therefore 1627.10 meters.

4.3 Flight Score

TABLE 4.1: Vehicle Performance Parameters

Parameter	Value
Cruise Mach Number	2.3
L/D Ratio	2.5
Payload Fraction	0.069
Flight Score	0.39675

4.4 Stability Analysis

4.4.1 Aerodynamic Parameters

The Aerodynamic Parameters obtained as a result of Aerodynamic Analysis are given below:

4.4.2 Static Stability

4.4.2.1 Longitudinal Stability

Static stability is a fundamental requirement in aircraft design, ensuring that the vehicle naturally returns to its trimmed condition following a small disturbance. For any design, achieving adequate static stability across a wide range of Mach numbers and altitudes is

vital to maintain control authority and reduce control system workload, especially during high-speed missions. This static stability analysis in this subsection is performed by evaluating the trim angle of attack and elevator deflection required for level flight at different Mach numbers and altitudes. The results offer key insights into the longitudinal stability characteristics of the UCAV across its flight envelope, helping ensure safe and responsive behavior in both cruise and maneuvering flight.

The Lift Coefficient for Cruise is given as:

$$C_{L_{cruise}} = \frac{W}{\frac{1}{2}\rho_{cruise} V_{cruise}^2 S_w} = 0.6657$$

We Know that,

$$\begin{aligned} \text{Downwash at } 0^\circ \text{ AoA: } \varepsilon_0 &= \frac{2C_{L_{0w}}}{\pi e A R_w} = 0.0865 \\ \text{Downwash gradient: } \frac{d\varepsilon}{d\alpha} &= \frac{2C_{L_{\alpha w}}}{\pi e A R_w} = 0.6455 \text{ rad}^{-1} \end{aligned}$$

The total lift characteristics are:

$$\begin{aligned} C_{L_0} &= C_{L_{0w}} + \eta_t \left(\frac{S_t}{S_w} \right) C_{L_{\alpha t}} (i_t - \varepsilon_0) = 0.2449 \\ C_{L_\alpha} &= C_{L_{\alpha w}} + \eta_t \left(\frac{S_t}{S_w} \right) C_{L_{\alpha t}} \left(1 - \frac{d\varepsilon}{d\alpha} \right) = 5.2881 \text{ rad}^{-1} \end{aligned}$$

Note: The Charactersitics of the V-Tail have been combined into an equivalent Horizontal and Vertical tail to ease analysis.[refer to [14]]

Thus, the cruise angle of attack is:

$$\alpha_{cruise} = \frac{C_{L_{cruise}} - C_{L_0}}{C_{L_\alpha}} = 0.0177 \text{ rad} = 1.01^\circ$$

Pitching Moment Characteristics:

$$\begin{aligned} C_{m_0} &= C_{m_{acw}} + C_{L_{0w}} (x_{CG} - x_{ac}) - \eta_t \left(\frac{S_t}{S_w} \right) C_{L_{\alpha t}} (i_t - \varepsilon_0) (x_{act} - x_{CG}) = +0.1551 \\ C_{m_\alpha} &= C_{L_{\alpha w}} (x_{CG} - x_{ac}) - \eta_t \left(\frac{S_t}{S_w} \right) C_{L_{\alpha t}} \left(1 - \frac{d\varepsilon}{d\alpha} \right) (x_{act} - x_{CG}) = -0.8707 \text{ rad}^{-1} \end{aligned}$$

Note: Fuselage contributions and thrust effects are neglected, assuming the thrust line passes through the CG.

Given the elevator effectiveness parameter from reference data: - $\tau = 0.45$

$$C_{L_{\delta_e}} = \eta_t \left(\frac{S_t}{S_w} \right) \left(\frac{dC_{L_t}}{d\delta_e} \right) = 0.4062 \text{ rad}^{-1}$$

$$\frac{dC_{L_t}}{d\delta_e} = C_{L_{\alpha t}} \cdot \tau$$

Moment coefficient per elevator deflection:

$$C_{m_{\delta_e}} = -V_H \cdot \eta_t \cdot \left(\frac{dC_{L_t}}{d\delta_e} \right) = -1.679 \text{ rad}^{-1}$$

To achieve trim at cruise:

$$\delta_{trim} = -\frac{C_{m_0} C_{L_\alpha} + C_{m_\alpha} C_{L_{cruise}}}{C_{m_{\delta_e}} C_{L_\alpha} - C_{m_\alpha} C_{L_{\delta_e}}} = +0.053 \text{ rad} = +3.54^\circ$$

$$\alpha_{trim} = -\frac{C_{L_{cruise}} - C_{L_{\delta_e}} \delta_{trim}}{C_{L_\alpha}} = 0.035 \text{ rad} = 1.15^\circ$$

These results confirm the adequacy of the volume distribution and demonstrate that the aircraft is statically stable in pitch.

Now, this process is automated for the cruise altitude input and variation in Trim Angle of Attack and Elevator Deflection is shown in figure 4.18.

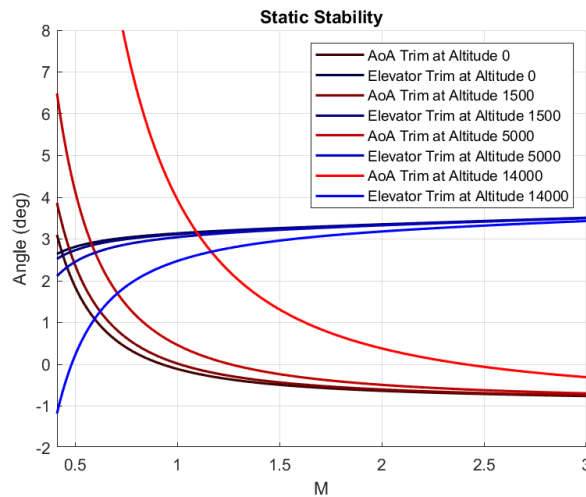


FIGURE 4.18: Trim Conditions

4.4.2.2 Directional Stability (Weathercock Stability)

Considering the side force contributions:

$$C_{n_{\beta wf}} = -K_n K_{RL} \left(\frac{S_{fuse}}{S_w} \right) \left(\frac{l_{fuse}}{b} \right) = -0.1127$$

Where:

$$K_n = 0.04, K_{RL} = 1.2$$

Vertical tail contribution:

$$C_{n_{\beta v}} = V_{VT} \cdot C_{L_{\alpha_{VT}}} \cdot n_t \left(1 + \frac{d\sigma}{d\beta} \right) = +0.3735$$

Using:

$$n_{VT} \left(1 + \frac{d\sigma}{d\beta} \right) = 0.724 + \frac{3.06(S_{VT}/S)}{1 + \cos \Lambda_{c/4}} + 0.4 \cdot \frac{Z_w}{d} + 0.009 A R_w = 1.447$$

Since,

$$C_{n_{\beta v}} > -C_{n_{\beta wf}},$$

The aircraft exhibits positive lateral static stability.

4.4.3 Dynamic Stability

This subsection analyses the dynamic stability of the aircraft. A highly stable aircraft would come back to its steady state after some initial disturbance.

The moments of inertia are estimated by following the process mentioned in [refer [\[4\]](#)]. The Approximations for each mode are referred to from (refer [\[15\]](#)).

4.4.3.1 Longitudinal Modes

The Phugoid (Long Period) mode is approximated by the following equation:

$$\begin{bmatrix} \Delta \dot{u} \\ \Delta \dot{\theta} \end{bmatrix} = \begin{bmatrix} X_u & -g \\ \frac{-Z_u}{u_0} & 0 \end{bmatrix} \begin{bmatrix} \Delta u \\ \Delta \theta \end{bmatrix} \quad (4.1)$$

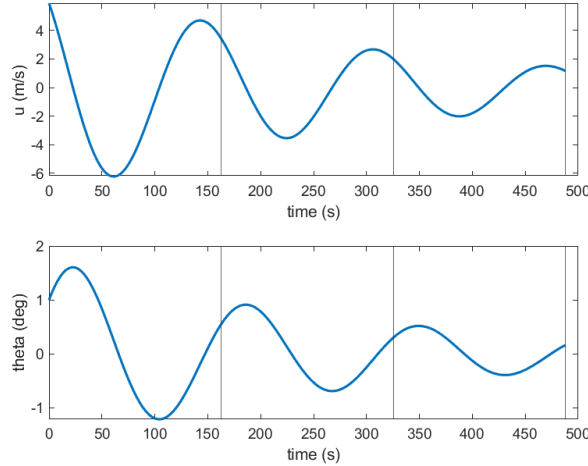


FIGURE 4.19: Phugoid Mode

The Phugoid motion time period is found to be 162.65s.

The Short Period mode is approximated by the following equation:

$$\begin{bmatrix} \Delta \dot{w} \\ \Delta \dot{q} \end{bmatrix} = \begin{bmatrix} Z_w & u_0 \\ M_w + M_{\dot{w}} Z_w & M_q + M_{\dot{w}} u_0 \end{bmatrix} \begin{bmatrix} \Delta w \\ \Delta q \end{bmatrix} \quad (4.2)$$

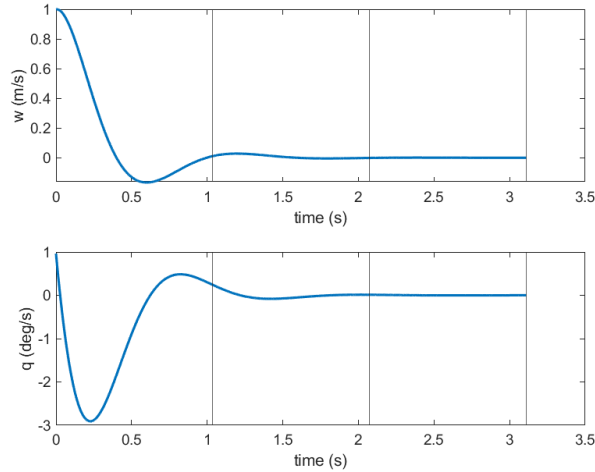


FIGURE 4.20: Short Period Mode

The Short Period motion time period is found to be 0.165s.

4.4.3.2 Lateral-Directional Modes

The Spiral Divergence Eigenvalue is found by the equation:

$$\lambda_{\text{spiral}} = \frac{L_\beta N_r - L_r N_\beta}{L_\beta} \quad (4.3)$$

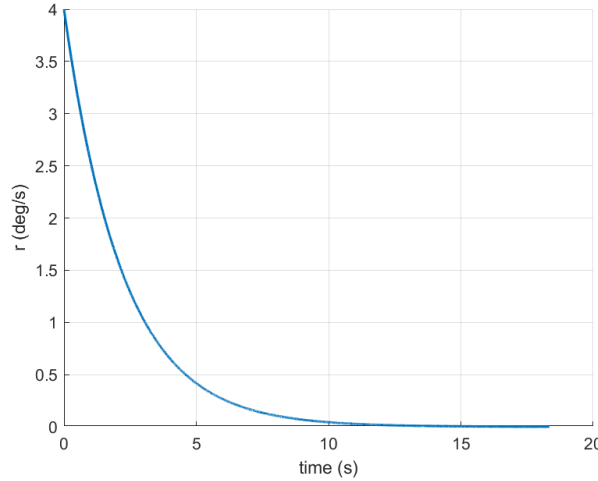


FIGURE 4.21: Spiral Divergence Mode

The value of eigenvalue is -0.4521. The negative value means that the disturbance is reduced exponentially over time.

The Eigenvalue for Roll Approximation is given by:

$$\lambda_{\text{roll}} = L_p \quad (4.4)$$

The value of eigenvalue is -1.1909. The negative value means that the disturbance is reduced exponentially over time.

Dutch Roll Approximation is given by:

$$\begin{bmatrix} \Delta\dot{\beta} \\ \Delta\dot{r} \end{bmatrix} = \begin{bmatrix} \frac{Y_\beta}{u_0} & -\left(1 - \frac{Y_r}{u_0}\right) \\ N_\beta & N_r \end{bmatrix} \begin{bmatrix} \Delta\beta \\ \Delta r \end{bmatrix} \quad (4.5)$$

The time period for dutch roll motion is 0.8551s.

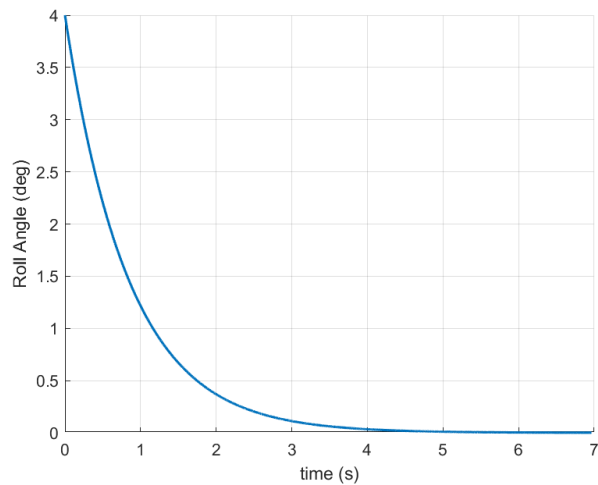


FIGURE 4.22: Roll Mode

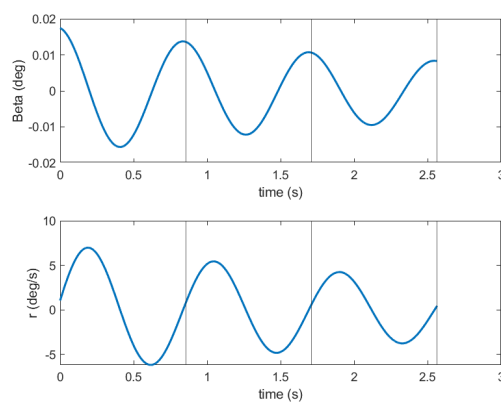


FIGURE 4.23: Dutch Roll Mode

Chapter 5

Structures and Loads

5.1 Introduction

This section discusses the various types of loads encountered by a UCAV during flight, including inertial loads, aerodynamic forces, and powerplant-induced loads. It also outlines the development of the flight envelope through the construction of a V-n diagram, which defines the operational limits of the aircraft. Additionally, a preliminary panel method is introduced to compute the lift distribution along the wing span. This distribution is then used to evaluate internal structural loads such as shear forces and bending moments. Based on these load calculations, the wing is appropriately sized to ensure structural integrity throughout the flight envelope.

5.2 Loading

The important types of loads that the aircraft experiences are majorly :

- Airloads due to gusts and high-g maneuvers
- Inertial loads which can be accelerations, vibration and flutter
- Powerplant loads causing thrust and torque
- Other loads during takeoff and landing .

In a typical maneuver load the supersonic UCAV is designed to limit load factors of +4 g and -2 g loadings . For a UCAV the ultimate load factor is considered to be 1.25 .

V-n diagram in figure 5.1 which depicts the aircraft limit load factor as a function of airspeed consists of parameters that we select including maximum positive load factor , most negative load facotr and maximum dive speed . It shows the loads and the gust velocities the aircraft must withstand.

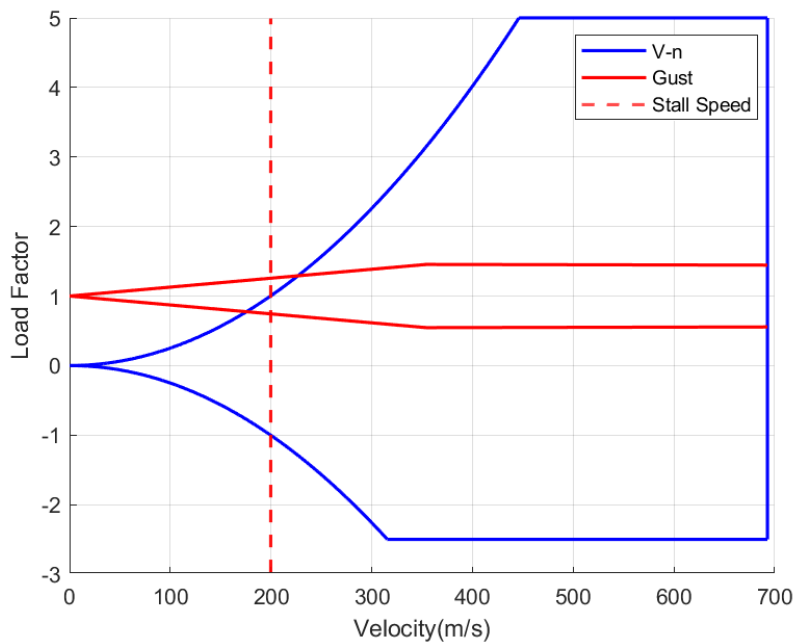


FIGURE 5.1: V-n diagram

Once the V-n diagram is depicted the actual loads and load distribution on the lifting surfaces such as the wing needs to be determined . The case highlighted here is at the max q velocities and any velocities where the gust load factor exceeds the assumed limit load factor. Classical wing theory for spanwise lift or load distribution is used for a non elliptical wing using Schrenk's approximation, which assumes This method assume. that the load distribution on an untwisted wing or tail has a shape that the average of the actual planform shape and an elliptic shape of the samespan and area . Considering the wing of a trapezoidal chord of equation :

$$C(y) = C_r \left[1 - \frac{2y}{b} (1 - \lambda) \right] \quad (5.1)$$

where

$$S = \frac{b}{2} C_r (1 + \lambda) \quad (5.2)$$

Since now the load applied is considered for initial calcuation as above the Shear force and Bending moment diagrams for the spanwise lift distribution is given in the figure 5.2 and 5.3

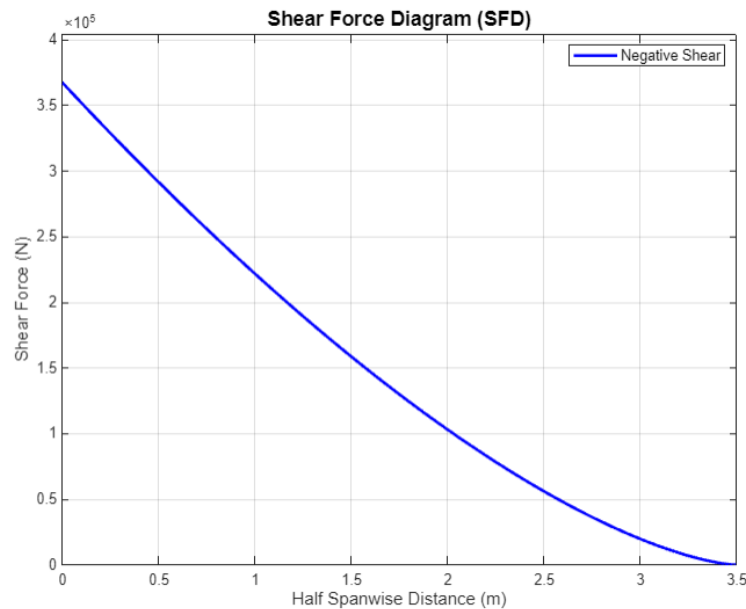


FIGURE 5.2: Shear Force Diagram

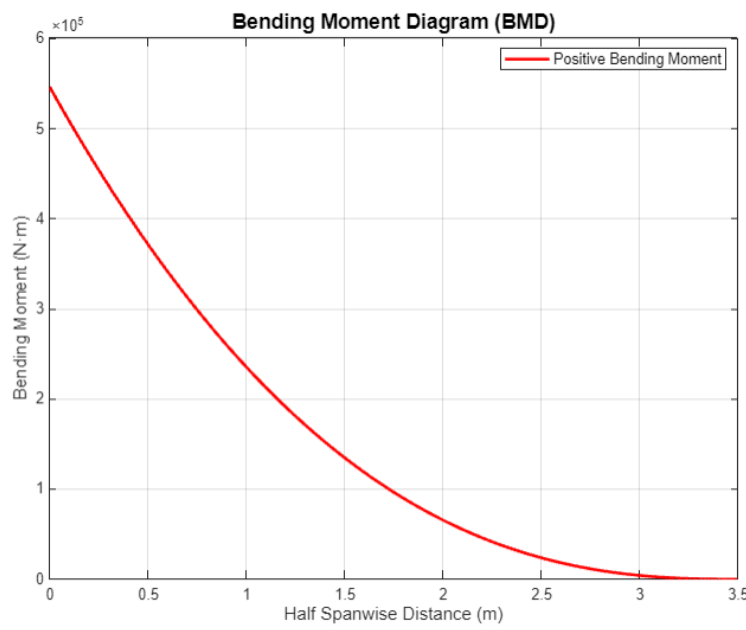


FIGURE 5.3: Bending Moment Diagram

5.3 Material Selection and Thermal Considerations

The selection of material for the design must be based on the sound engineering principles and a small mistake in the design of aircraft's fuselage , skeleton wing or any critical part can be fatal. The important material selection consideration for the UCAV includes :

- Specific Strength (Strength to Weight Ratio)
- Tensile Mechanical Properties
- Fatigue Strength
- Low Speed Impact Strength
- Resistance to stress corrosion & crack propagation
- Resistance to creep

The supersonic UCAV's skin temperature is a function of its speed and environment. The skin temperature drops initially as the aircraft climbs due to exposure to decreasing ambient air temperatures. As the speed increases above about Mach 1, where the temperature begins to increase, the skin temperature reaches a maximum of 120 °C (248 °F) [16] after exposure while cruising at Mach 2.2. (At Mach 2.0, the skin temperature would stay below 100 °C (212 °F); at Mach 2.4, it would reach 150 °C (302 °F.) During descent, the reverse occurs.

Cruising at speed around 2.3 Mach, requires a material resistant to longterm creep at temperatures ranging from 100 to 130 °C. A suitable cost-effective material, for this application, may be the 2650 aluminum alloy; which presents such properties at relatively high temperatures ($130 \text{ }^{\circ}\text{C} = 0.43T_{\text{melting}}$) [17] [18]. Exposure to temperatures ranging from 100 to 130 °C during the supersonic flying phase, using the 2650-T8 alloy in figure [16], showed that the material did not deform by more than 0.1 % under a 150 MPa stress.

So for the current UCAV the materials involved in terms of airframe which includes fuselage , wing are given in the below table 5.1 :

5.4 Wing Structure

Wing structure depicts the outline of the wing both in planform and cross-sectional shape , they must be suitable for housing a structure capable of handling the shear and bending

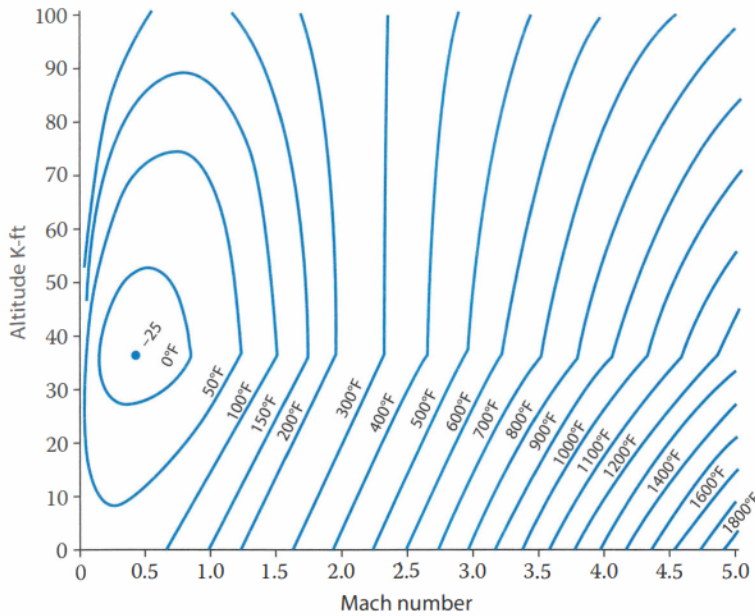


FIGURE 5.4: Temperature distribution at different altitudes to mach number

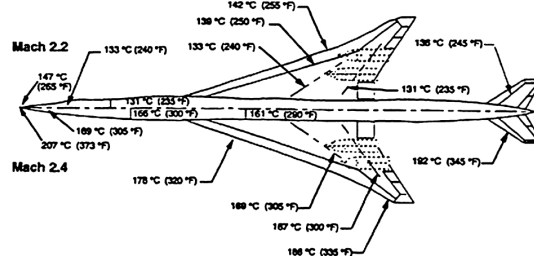


FIGURE 5.5: Predicted equilibrium skin temperatures for Mach 2.2 and 2.4 SCT aircrafts

TABLE 5.1: Material properties of aircraft structural components

Component	Material	Density (g/cm³)	Tensile Strength (MPa)	Young's Modulus (GPa)	Operating Temp. Limit (°C)
Fuselage Skin	PMR-15 (CFRP)	1.6	1000-1600	140-160	315-350
Skeleton	Ti alloy	4.43	900-1100	110	400-600
Wing Skin	High strength CFRP	1.6	1200-1800	150-180	120-350
Rib	Al 2650 T8 alloy	2.75	480-510	72-76	120-150
Spar	Ti-6Al-4V	4.43	900-1000	110	400-550

loads . For the current UCAV design it consists of a multi spar box structure for lower aspect ratio wing since it uses a thin wing airfoil . The current structure consists of a delta wing hence requires it is of converging spars configuration [5.6](#) for the wing box .

The UCAV now [5.7](#) consists of 18 number of ribs for the whole span(9 at each side) and at a equidistant spacing of 0.435 m calculated for a preliminary design [19] .The spacing is optimized according to the figure and consists of 3 spars mainly the front spar at 25% location of chord , intermediate spar at 45% location of the chord and rear spar at the

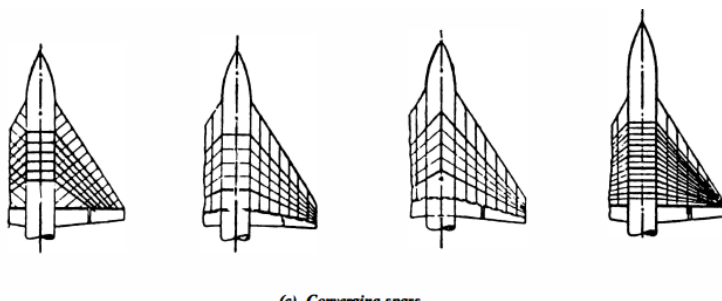
(c) *Converging spars*

FIGURE 5.6: Converging Spars [19]

65% of the spar . The spar cross section consists of a I beam cross section since it can handle huge bending loads at higher speeds .

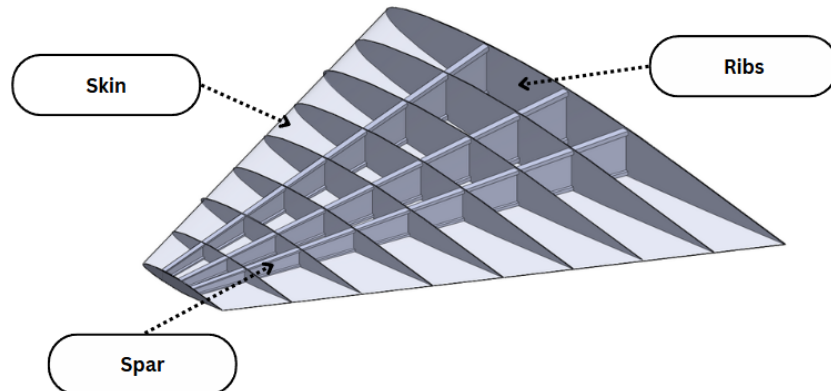


FIGURE 5.7: Wing Structure

Chapter 6

Propulsion Sizing

6.1 Background

The propulsion system is a critical component that must be carefully considered during the conceptual design phase of an aircraft. It influences the vehicle's mission capabilities, aerodynamic configuration, operational envelope, and overall system performance. The selection of an extreme engine thrust to meet one mission requirement may limit another, hence a compromise is necessary. In this chapter, we focus on scaling the available engines to provide the thrust necessary to overcome the drag based on the different mission requirements.

Conceptual design of Supersonic unmanned combat aerial vehicle (SUCAV) requires supersonic speed and different engines behave differently at different speeds so there is a need to check which engine is suitable as per our requirements. After selecting the engine, a cross-verification is also required between the total thrust estimated from the cycle analysis and the actual thrust rating of the selected engine.

6.2 Engine Sizing

After selecting turbojets with afterburner , the different configurations possible within the turbojets are shown in the table [6.1](#)

TABLE 6.1: Comparative Performance Specifications of Jet Engines

Parameter	AL-7F	R-29	AL-21F3	JT4A-11	Olympus 593	J93-GE-3
Type	A/B turbojet	Turbojet	A/B turbojet	Turbojet	Turbojet	A/B turbojet
Thrust (kN)	67.1	78.5	76.4	77.8	139.4	98.0
Weight (kg)	2,010	1,880	1,700	2,313	3,175	2,300
Pressure ratio	9.5:1	12.9:1	14.8:1	12.5:1	82:1	—
Temp. (K)	1,133	1,356	1,373	—	—	1,422
SFC (kg/(h·kW))	98.9	96.8	87.7	75.6	121.7	71.3
T/W Ratio	3.4	4.45	4.6	3.15	5.4	6.0

The determination of the required engine thrust was performed using the thrust loading versus wing loading graph in conjunction with the estimated maximum take-off weight of the aircraft. Based on the aerodynamic constraints and mission profile—which includes cruise at Mach 2 and an altitude of 14 km—the target thrust-to-weight ratio was selected. From there we find the total thrust required and then matched with the above given configurations. After evaluating the engine which satisfy our requirements was Tumansky R-29 engine [20].

6.3 Cycle Analysis

Cycle analysis is the stage where one evaluates how efficiently the engine has been selected . It also allows us to determine the total thrust and specific fuel consumption (SFC) generated by the engine. Ideal turbojets analysis are easy to perform but they are not realistic. The following analysis is performed for an actual turbojet engine without an afterburner. The turbojet engine consists of a diffuser, a compressor, a burner, a turbine and a nozzle. Schematic drawing of a turbojet engine is as shown below figure 6.1 :

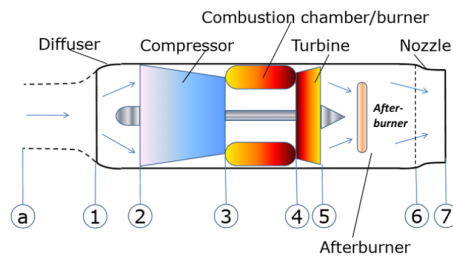


FIGURE 6.1: Engine Cycle

The general parameters used for calculating the total thrust is taken from the reference book of mechanics and thermodynamics [21]. The engine analysis is done at an altitude of 14km where ambient pressure and temperature are $1.538e4$ Pa and 212 K. The selected

engine was Tumansky R-29. In cycle analysis, we get the temperature and pressure at the outlet of each component [6.2](#). Subsequently, it is necessary to verify whether the nozzle is choked or not. In our case, based on the given parameters, it is found that the nozzle is choked. Then we calculate the total thrust with the help of the below equation :

$$\mathcal{T} = \dot{m}_a [(1 + f) u_e - u] + (p_e - p_a) A_e \quad (6.1)$$

where,

- \mathcal{T} = total thrust
- F = fuel ratio
- u_e = exit velocity
- u = Inlet velocity
- P_e = exit pressure
- P_a = ambient pressure
- A_e = area of the exit

Component	Adiabatic efficiency	Average specific heat ratio
Diffuser	$\eta_d = 0.97$	1.40
Compressor	$\eta_c = 0.85$	1.37
Burner	$\eta_b = 1.00$	1.35
Turbine	$\eta_t = 0.90$	1.33
Nozzle	$\eta_n = 0.98$	1.36
Fuel heating value, 45,000 kJ/kg		
Flight altitude (cruise Mach no.)	Ambient pressure (kPa)	Ambient temperature (K)
Sea level (0)	101.30	288.2
40,000 ft (12,200 m) (0.85)	18.75	216.7
60,000 ft (18,300 m) (2.0)	7.170	216.7
80,000 ft (24,400 m) (3.0)	2.097	216.7

FIGURE 6.2: Component efficiency

After doing the regular cycle analysis of actual turbojet engine, the total thrust that came out was 70.147 KN which is a good estimation according to the given total thrust from the table (78.48KN). So the selection of our engine was quite a good approximation.

Chapter 7

Radar Cross Section(RCS)

7.1 Background

Since the use of military aviation, there is a very high demand of low detectable aircraft . One of the main parameters concerning low observability is radar cross section (RCS), which is a measure of the amount of energy reflected by a target in a particular direction when it is illuminated by electromagnetic waves. Radar systems are placed to detect the objects by transmitting the electromagnetic (EM) waves signal to the object and when these waves strike the surface of an aircraft, a portion of the signal is reflected back to the radar receiver, enabling the detection and tracking of the object. As technology increases day by day, more advancements can be seen in developing a very low detectable aircraft.

7.2 RCS Analysis

Here for the numerical calculation of rcs [22], we use Physical optics method which works good for low to moderate fidelity. POFACETS is a physical optics approximation Matlab®-based code that discretizes the geometry into triangular facets and computes the total signature by superposition of scattering resulting from the illuminated facets [23], including the effects of different materials and ground plane [24] .Till now RCS have been calculated only for monostatic radar. After placing my model (in .stl file) into the Matlab , the rcs came out to be -35 dBsm (0.00030736 m^2). The rcs vs azimuth angle can be seen as in figure 7.1. The flucations vary from -54 dBsm to -60 dBsm.

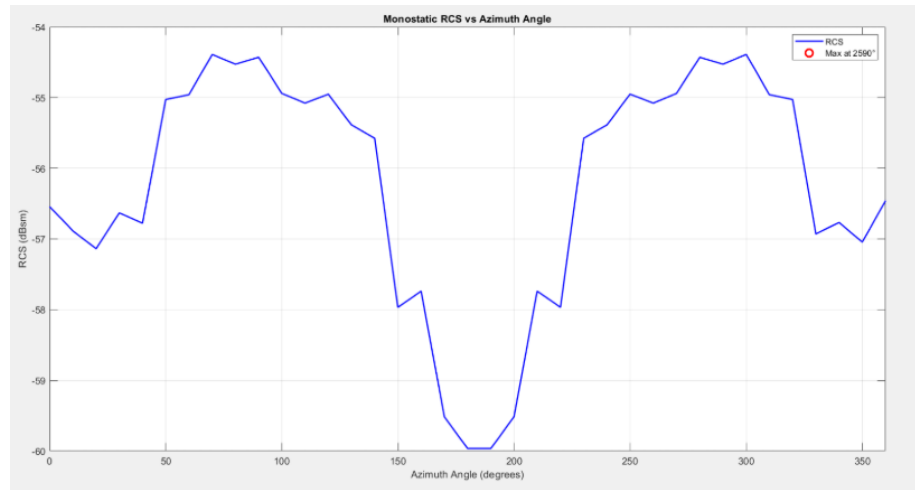


FIGURE 7.1: Monostatic RCS v/s Azimuth Angle

Additionaly to get stealth RAM coatings are applied such as iron ball paints on the surface so that it reduces rcs. And RAM converts incoming radar energy into heat through dielectric loss or magnetic loss, rather than allowing it to reflect back to the radar receiver.

Chapter 8

Conclusion

This phase of the project has successfully achieved a comprehensive conceptual design and analysis of a supersonic unmanned combat aircraft, focusing on wing optimization, structural integrity, aerodynamics, performance, stability and propulsion sizing. The optimized wing sizing, combined with weight estimation and aerodynamic analysis using a lower-order supersonic model, has demonstrated satisfactory performance across both subsonic and supersonic flight regimes. Notably, the aircraft exhibits slightly improved static stability at supersonic speeds, consistent with theoretical expectations. The overall weight remains within an acceptable and realistic range for the design mission.

The OpenMDAO framework has proven to be a robust and flexible platform for multidisciplinary analysis and optimization, providing a solid foundation for maximizing overall flight performance. Structural design efforts have resulted in a completed internal wing structure, supported by appropriate material selection and validated through the development of a V-n diagram, ensuring compliance with structural load requirements.

Engine sizing has also been completed in alignment with the mission profile and aerodynamic characteristics. However, due to the aerodynamic model being primarily tuned for supersonic flow, the wing demonstrates reduced efficiency in subsonic conditions. Addressing this limitation will be a key focus in future work.

Subsequent development will involve enhancing the aerodynamic model accuracy, particularly in the subsonic regime, through the integration of higher-fidelity tools. Additionally, RANS-based CFD simulations will be performed on the final refined configuration to validate aerodynamic predictions and support further refinement.

Bibliography

- [1] “OpenVSP.” <https://openvsp.org/>.
- [2] V. Ahuja and R. J. Hartfield, “Aerodynamic loads over arbitrary bodies by method of integrated circulation,” *Journal of Aircraft*, 2016.
- [3] J. S. Gray, J. T. Hwang, J. R. R. A. Martins, K. T. Moore, and B. A. Naylor, “Openmdao: An open-source framework for multidisciplinary design, analysis, and optimization,” *Structural and Multidisciplinary Optimization*, 2019.
- [4] D. P. Raymer, *Aircraft Design: A Conceptual Approach*. Reston, VA: AIAA Education Series, 5th ed., 2012.
- [5] J. Anderson, *Aircraft Performance & Design*. McGraw-Hill international editions, McGraw-Hill Education, 1999.
- [6] M. H. Sadraey, *Aircraft Performance: An Engineering Approach*. Hoboken, NJ: Wiley, 2017.
- [7] S. Farokhi, *Aircraft Propulsion*. Hoboken, NJ: Wiley, 1st ed., 2008.
- [8] R. C. Nelson, *Flight Stability and Automatic Control*. McGraw-Hill Aerospace Engineering Series, McGraw-Hill Education, 2 ed.
- [9] B. Etkin, *Dynamics of Flight: Stability and Control*. Wiley Professional Aviation Series, John Wiley & Sons, 3rd ed., 1996. Classic text on aircraft flight dynamics.
- [10] C. D. Perkins and R. E. Hage, *Aircraft Performance, Stability and Control*. John Wiley & Sons, 1st ed., 1949. The classic reference on aircraft performance and handling qualities.
- [11] R. W. Saaty, “The analytic hierarchy process—what it is and how it is used,” *Mathematical Modelling*, vol. 9, no. 3–5, pp. 161–176, 1987.

- [12] S. Pugh, *Total Design: Integrated Methods for Successful Product*. Cambridge, UK: Cambridge University Press, 1st ed., 1991.
- [13] S. Gudmundsson, *General Aviation Aircraft Design*. Vancouver, Canada: Excellent Publishing, 2016.
- [14] F. Nicolosi, P. Della Vecchia, and D. Ciliberti, “A comprehensive review of vertical tail design,” in *Aerospace Europe – 6th CEAS Conference*, (Hamburg, Germany), June 2016. Available at https://www.fzt.haw-hamburg.de/pers/Scholz/ewade/2016/Paper_FNicolosi.pdf.
- [15] R. Nelson, *Flight Stability and Automatic Control*. McGraw-Hill aerospace science & technology series, McGraw-Hill Education, 1998.
- [16] Z. Huda and P. Edi, “Materials selection in design of structures and engines of supersonic aircrafts: A review,” *Materials & Design*, vol. 46, pp. 552–560, 2013.
- [17] J. C. Williams and E. A. Starke Jr, “Progress in structural materials for aerospace systems,” *Acta Materialia*, vol. 51, no. 19, pp. 5775–5799, 2003.
- [18] J. Majimel, M. J. Casanove, and G. Molénat, “A 2xxx aluminum alloy crept at medium temperature: Role of thermal activation on dislocation mechanisms,” *Materials Science and Engineering: A*, vol. 380, no. 1–2, pp. 110–116, 2004.
- [19] Y. Niu, Michael C. and M. Niu, *Airframe Structural Design: Practical Design Information and Data on Aircraft Structures*. Hong Kong; Granada Hills, CA, USA: Commilit Press (distributed by Adaso/Adastra Engineering Center), 2nd ed., 1999.
- [20] B. Gunston, *World Encyclopedia of Aero Engines*. Cambridge, England: Patrick Stephens Limited, 1989.
- [21] P. G. Hill and C. R. Peterson, *Mechanics and Thermodynamics of Propulsion*. Reading, MA: Pearson, 2nd ed., 1991.
- [22] E. Sepulveda, H. Smith, and D. Szirocki, “Multidisciplinary analysis of subsonic stealth unmanned combat aerial vehicles,” *CEAS Aeronautical Journal*, vol. 9, no. 1, pp. 47–62, 2018.
- [23] E. J. Garrido, “Graphical user interface for a physical optics radar cross section prediction code,” Master’s thesis, Naval Postgraduate School, Monterey, California, 2000.

- [24] F. Chatzigeorgiadis, “Development of code for a physical optics radar cross section prediction and analysis application,” Master’s thesis, Naval Postgraduate School, Monterey, California, 2004.
- [25] W. Green and G. Swanborough, *The Great Book of Fighters*. St. Paul, Minnesota: MBI Publishing, 2001.
- [26] “The development of aircraft power plant construction in the ussr and the 60th anniversary of ciam,” in *AIAA/ASME/SAE/ASEE 26th Joint Propulsion Conference*, (Orlando, Florida), July 1990. AIAA-90-2761.
- [27] A. F. El-Sayed, *Aircraft Propulsion and Gas Turbine Engines*. CRC Press. Check publisher/year if not CRC or missing.
- [28] “Rolls royce snecma olympus,” *Janes Transport News*.
- [29] “Data on large turbofan engines.” Technical report or dataset; further info needed.
- [30] J. W. Taylor, *Jane’s All the World’s Aircraft 1962–63*. London: Sampson, Low, Marston & Co Ltd, 1962.
- [31] S. I. Jaffery and P. T. Mativenga, “Assessment of the machinability of ti-6al-4v alloy using the wear map approach,” *International Journal of Advanced Manufacturing Technology*, vol. 40, no. 7-8, pp. 687–696, 2009.
- [32] V. P. McConnell, “Resins for the hot zone, part ii: Bmis, ces, benzoxazines and phthalonitriles.” *High-Performance Composites*, September 2009, 2009. <http://www.compositesworld.com>.